Naval Research Reviews

Office of Naval Research
Two/1998
Vol L

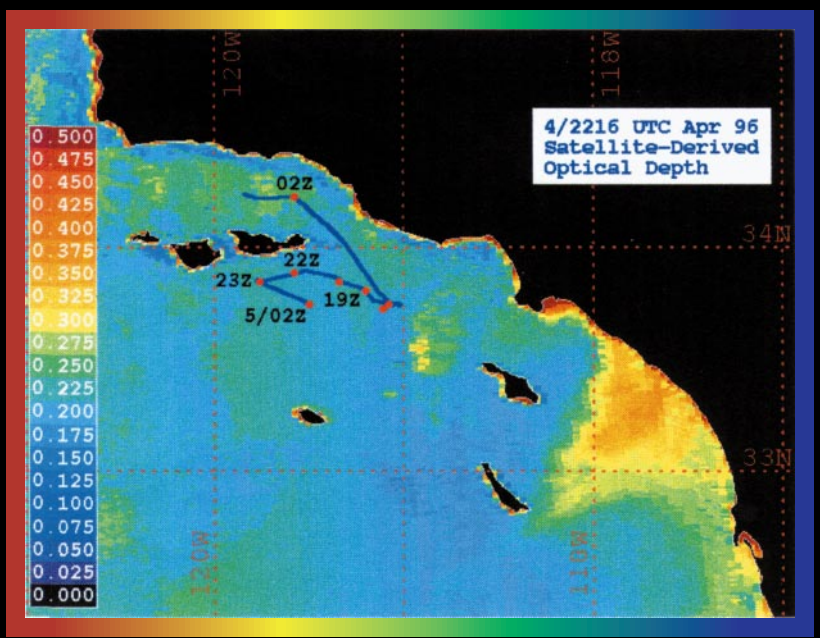

Coastal Meteorology and Oceanography

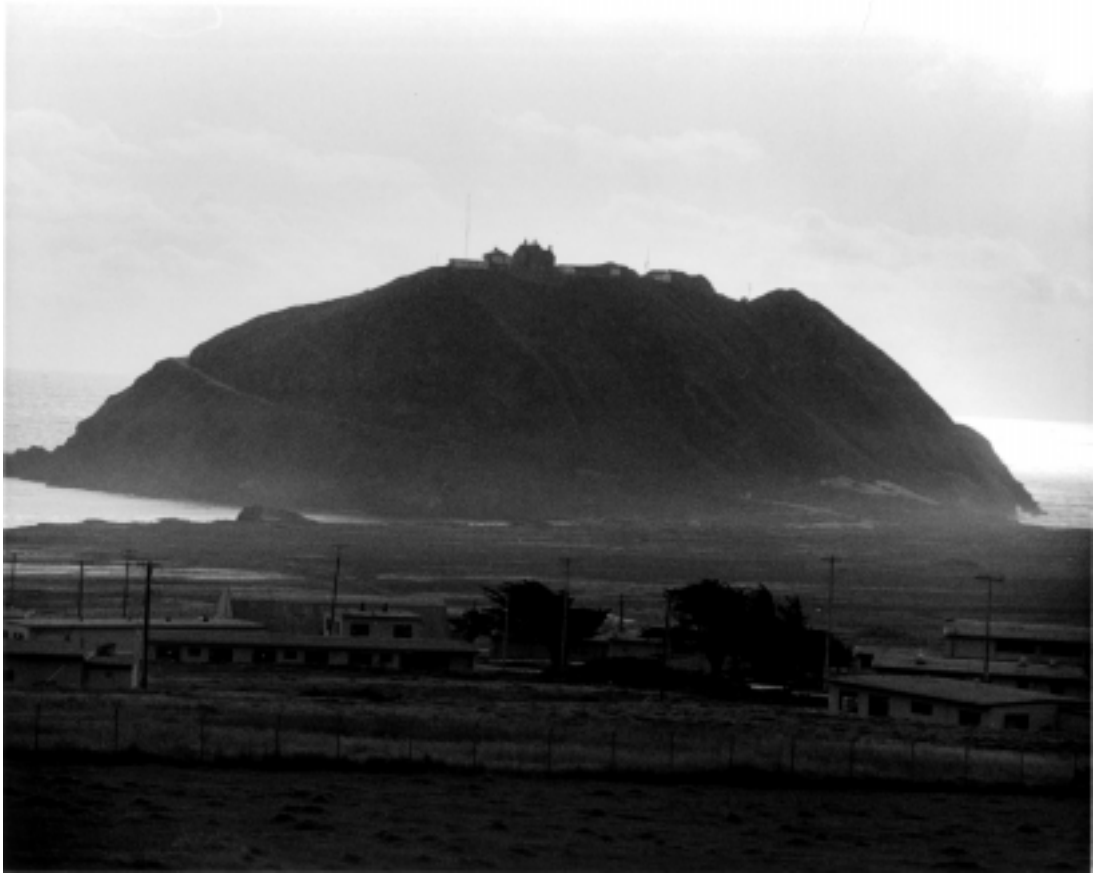

Site of the Naval Postgraduate School Ocean Acoustic Observatory.
Located at the scenic Pt. Sur, California, the Observatory operates a former US Navy shore-based surveillance hydrophone array to advance basic and applied research in acoustical oceanography and underwater acoustics. In partnership with both internal and external investigators, the Coastal Ocean Acoustics Center at the Naval Postgraduate School is actively employing the Observatory to study the California coastal circulation acoustically, the behavior and distribution of vocalizing marine mammals, and the physics of sound propagation in a complex littoral environment. The Observatory also supports a meteorological station as part of the Real-Time Environmental Information Network and Analysis System project. Most of the ongoing research at the Observatory is sponsored by the Office of Naval Research. For more information, see http:// www.usw.nps.navy.mil/ptsur.

Naval Research Reviews

Office of Naval Research
Two/1998
Vol L

Articles

2
Describing Coastal Optical Properties with in situ and Remote Measurements
K. L. Davidson and C. H. Wash

8
Simulation of Drifters in a Turbulent Ocean
R. W. Garwood, Jr., R. R. Harcourt, and R. E. Stone

13
Megaripples in the Nearshore
E. B. Thornton, E. L. Gallagher, and T. P. Stanton

20
Subsurface Lagrangian Measurements in the Northeastern Pacific Ocean
C. Collins, N. Garfield, R. Paquette, T. Rago, and E. Carter

24
The Real-Time Environmental Information Network and Analysis System (REINAS)
W. A. Nuss, D. D. E. Long, P. E. Mantey, A. Pang, E. C. Rosen, and J. Paduan

31
Toward Accurate Coastal Ocean Prediction
P. C. Chu

Departments

19
Profile in Science

About the cover
The influence of aerosols, important in the assessment of performance of electro-optical sensors in the atmosphere, is estimated from NOAA satellite data off the Southern California coast. Land areas are masked as black. Color scale depicts aerosol influences and isolates a plume of continental aerosols directed off-shore between San Diego and Los Angeles. The track of the R/V Point Sur with in-situ sensors is indicated during the March 1996 Intensive Observation Period of the EO Propagation Assessments in Coastal Environments (EOPACE) project. Please see article by Davidson and Wash on page 2.

Naval Research Reviews publishes articles about research conducted by the laboratories and contractors of the Office of Naval Research and describes important naval experimental activities. Manuscripts submitted for publication, correspondence concerning prospective articles, and changes of address, should be directed to Code 00PA, Office Naval Research, Arlington, VA 22217-5660. Requests for subscriptions should be directed to the Superintendent of Documents, U.S. Government Printing Office, Washington, DC 20403. *Naval Research Reviews* is published from appropriated funds by authority of the Office of Naval Research in accordance with Navy Publications and Printing Regulations. NAVSOP-35.

Describing Coastal Optical Properties with in situ and Remote Measurements

Kenneth L. Davidson and Carlyle H. Wash, Department of Meteorology, Naval Postgraduate School, Monterey, CA

Introduction

Knowledge of the coastal Marine Atmospheric Boundary Layer (MABL) is critical for modern Navy operations. To support modern weapon and sensor systems, quantitative assessment of a number of MABL properties are needed. The properties include: optical depth, near-surface optical turbulence, aerosol distribution, boundary layer depth, sea surface temperature, and surface layer temperature and moisture. These needs are even more critical in the coastal zone with the sparse surface observations away from the coast and the high temporal and spatial variability of littoral circulation systems.

The NPS Department of Meteorology objective is to enhance the capability to model near-surface optical propagation and refine remote sensing techniques to derive estimates of MABL properties. The Department has expertise with over water measurements and with processing and interpretation of satellite sensed data. We have deployed near-surface measurement systems on ships or buoys during several field experiments in which optical measurements were made. We have developed algorithms to estimate optical depth and other MABL properties from multispectral satellite data received at NPS.

Electro-optical propagation models, such as LOWTRAN, MODTRAN and IRTOOL, are formulated and evaluated based on field experiment data. The applicability of these models for coastal regions is not known. Existing models for optical turbulence were based on over land data. A deficiency exists in the formulation and evaluation of models which estimate near-surface optical conditions using measured bulk (mean) property parameters.

Satellite remote sensing provides an opportunity to measure MABL properties in the coastal zone with high spatial resolution. Algorithms using multispectral data from the polar orbiting and geostationary satellites to estimate MABL properties are being evaluated at NPS. Each polar orbiting NOAA satellite provides information at a given sunlit loca-

tion up to twice per day, but the GOES geostationary satellites provide nearly continuous daylight monitoring of equatorial and midlatitude coastal environments.

NPS meteorologists and equipment have participated in the EO Propagation Assessment in Coastal Environments (EOPACE) program, which is focused on the characterization of aerosol and boundary layer properties in the coastal zone. The near-surface measurement systems have been deployed and multispectral satellite data was collected during several Intense Observing Periods (IOPs) in 1996 and 1997. The purpose of this article is to highlight the results of using EOPACE data to evaluate optical turbulence modeling and the satellite algorithm to estimate optical depth.

Part A addresses the Optical Turbulence Modeling and part B will address the Satellite Optical Depth Retrieval.

A. Describing Optical Turbulence

Electro-optical (EO) propagation through the atmosphere near the ocean surface experiences rapid intensity fluctuations due to atmospheric turbulence, known as scintillation. Scintillation is closely related to the refractive index structure parameter, C_n^2. In an operational environment it would be useful to be able to evaluate and predict the effects of scintillation by estimating C_n^2 from routinely measured air-sea parameters. Bulk models have been developed to estimate near-surface atmospheric turbulence properties from mean meteorological measurements. The relations between other atmospheric turbulence properties and C_n^2 have also been established, thereby allowing C_n^2 to be estimated from mean air-sea measurements using existing turbulence scaling methods. The purpose of NPS collaborative studies in this area is to determine how accurately C_n^2 can be estimated from routine meteorological measurements using bulk models under various conditions.

During the Electro-Optical Propagation Assessment in a Coastal Environment (EOPACE) experiment of August-September 1997, infrared transmission measurements were obtained along a 7 km path over San Diego Bay. Simultaneous meteorological measurements were obtained from a buoy located at the midpoint of the transmission path. Bulk C_n^2 estimates computed from mean measurements obtained on a buoy are compared with concurrent optical transmission-derived C_n^2 measurements along an over-water propagation path to determine how closely the two methods agree under various air-sea conditions.

1. Background

The structure parameter for a quantity y is given by

$$C_y^2 = \frac{\overline{[y(x) - y(x+r)]^2}}{r^{2/3}}, \qquad (1)$$

where $y(x)$ and $y(x + r)$ are the values of parameter y at two points separated by a distance r along the mean wind direction and the over-bar indicates an ensemble average. The refractive-index structure parameter, C_n^2, can be expressed according to the structure parameters for temperature, C_T^2, humidity, C_q^2 and the temperature-humidity fluctuation correlation, C_{Tq}, as follows (Andreas [1]):

$$C_n^2 = A^2 C_T^2 + 2ABC_{Tq} + B^2 C_q^2, \qquad (2)$$

where the coefficients A and B are known functions of the wavelength (λ) and the mean atmospheric pressure (P), temperature (T), and specific humidity (q). The first term on the right hand side of Eq. (2) represents temperature fluctuations and is always positive, the second term represents the correlation of temperature and humidity fluctuations and can be positive or negative, while the third term represents humidity fluctuations and is always positive. For optical and infrared wavelengths the first term in Eq. (2) generally dominates, however, when the air-sea temperature difference is small the last two humidity-dependent terms can dominate.

Monin-Obukhov similarity (MOS) theory is used to relate the structure parameters C_T^2, C_q^2 and C_{Tq} in Eq. (2) to the mean properties of the atmospheric surface layer.

According to MOS theory, the surface layer scaling parameters T_*, q_* and u_* can be expressed in terms of the mean surface layer properties by the expression:

$$x_* = (\Delta x)k\left[\ln(z/z_{ox}) - \psi_x(\xi)\right]^{-1}, \qquad (3)$$

where x represents wind speed (u), temperature (T) or specific humidity (q) and the symbol Δ denotes the mean air-sea difference. The ψ functions are the integrated dimensionless profile functions, defined by Paulson [2]. When a dynamical property is properly scaled by the X_* parameters, it can be expressed as a universal function of ξ, defined as:

$$\xi = \frac{z}{L} = \frac{zkg(T_* + 0.61Tq_*)}{Tu_*^2} \qquad (4)$$

Here L is the Monin-Obukhov length scale, k is the von Karman constant (= 0.4) and g is the acceleration due to gravity. ξ is often referred to simply as the 'stability', and is negative in unstable conditions, zero in neutral conditions, and positive in stable conditions. The parameters z_{ou}, z_{oT} and z_{oq} are known as the 'roughness lengths,' and were determined by the bulk surface-layer model formulated by Fairall, et al. [3].

Structure parameters for temperature (C_T^2), the temperature-humidity correlation (C_{Tq}) and humidity (C_q^2) are properly scaled according to MOS theory, e.g.

$$C_T^2 = T_*^2 z^{-2/3} g_T(\xi), \qquad (5)$$

where g_T is a dimensionless function of ξ which must be

determined empirically. Observations have not conclusively demonstrated that these functions are different from each other and MOS theory implies they should be similar [4]. Measurements of g_T for highly stable conditions are rare and exhibit much scatter. In this study we have used the function for g_T given by Andreas [1].

2. In situ Coastal Experiment

An EOPACE IOP experiment took place in San Diego Bay in August-September 1997. Infrared (IR) transmission measurements were obtained by SPAWAR System Center, San Diego (SSC-SD). The transmission path was 7 km in length over San Diego Bay, with the IR source (transmitter) located at the Naval Amphibious Base and the IR receiver located at the Naval Submarine Base (see Figure 1). Meteorological data were obtained concurrently with the transmission data from an instrumented NPS buoy deployed at the mid-point of the transmission path.

Figure 1
EOPACE experimental setup, August-September 1997.

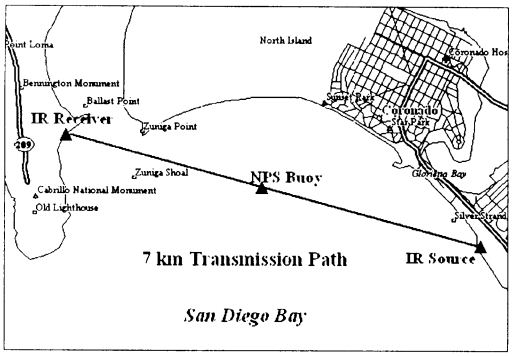

Wind speed, air temperature, humidity, atmospheric pressure, and sea temperature were measured on the NPS buoy. The buoy measurements were averaged over 10 minute intervals, and bulk estimates of height corrected C_n^2 were then computed from these mean values. The transmission measurements were obtained using instruments and procedures similar to those described by Zeisse, et al. [5]. The transmitter at the Amphibious Base was 6.2 m above mean sea level (MSL) and the receiver at the Submarine Base was 4.9 m above MSL. High-frequency mid-wave (3.5 to 4.1 μm) IR transmission measurements were obtained hourly. C_n^2 values were obtained by applying the normalized variance of the transmission data to the model formulated by Churnside et al. [6].

3. Bulk versus Transmission C_n^2 Comparisons

A scatter plot of the NPS bulk and SSC-SD transmission C_n^2 values is presented in Figure 2. A summary of the comparison statistics is presented in Table 1. The data have been separated into air-sea temperature difference (ΔT) intervals, as measured on the NPS buoy. The linear correlation coefficient between the two populations is presented in the second column. The '% difference' is the average value of $(C_{n\,(trans)}^2 - C_{n\,(bulk)}^2)/C_{n\,(trans)}^2$. The 'rms % difference' is the value of $[(C_{n\,(trans)}^2 - C_{n\,(bulk)}^2)^2]^{1/2}$, where the brackets denote an average, divided by the mean value of C_n^2(trans).

Figure 2
Scatter plot of transmission log(C_n^2) measurements versus bulk log(C_n^2) estimates separated into air-sea temperature difference (ΔT) intervals. Data points within the Bowen ratio (B_0) interval -0.1 < B_0 < -0.015 indicated by squares.

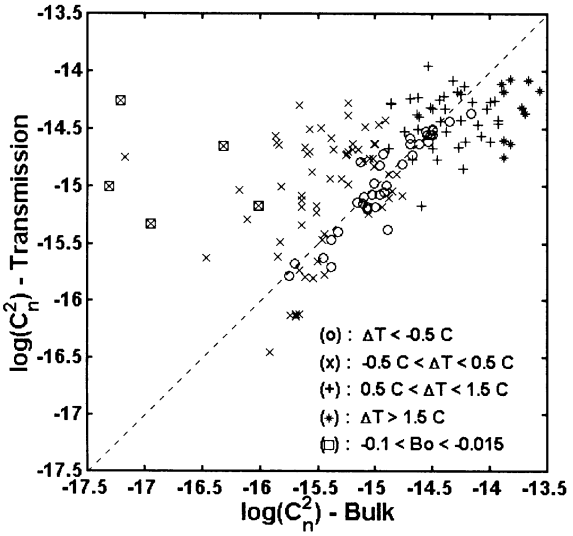

Bulk and transmission C_n^2 values agree very well for unstable conditions (ΔT < -0.5 °C). The agreement between is very poor for near-neutral conditions (-0.5 °C < ΔT < 0.5 °C), exhibiting a very large degree of scatter (rms % difference of 358%), with the bulk C_n^2 estimates being much lower than the transmission measurements in most cases. In near-neutral conditions bulk C_n^2 estimates are most sensitive to the measured values of ΔT and Δq. In weakly stable conditions (0.5 °C < ΔT < 1.5 °C), the comparison between the two methods exhibits much more scatter than for unstable cases. For strongly stable conditions (ΔT > 1.5 °C) the transmission C_n^2 measurements are systematically much lower than the bulk estimates, by 293% on average. There are several probable reasons for the poor accuracy observed in bulk C_n^2 estimates in stable conditions. These include the sensitivity to the measured values, that the dimensionless structure function parameter, g(ξ) is poorly

known, and that turbulence is severely suppressed by the atmospheric stratification, thereby invalidating MOS theory. It is also possible that the optical transmission data were 'saturated' for these very stable conditions, thereby causing the transmission values to be much lower than the bulk estimates.

Table 1
Bulk versus transmission C_n^2 comparison statistics.

ΔT Range	Corr Coeff	% Diff	rms % Diff
ΔT < -0.5 °C	0.93	-16	35
-0.5 °C < ΔT < 0.5 °C	-0.05	33	358
0.5 °C < ΔT < 1.5 °C	-0.02	-45	86
0.5 °C < ΔT	0.28	-293	228

A more complete discussion of the analysis results is available in Frederickson, et al [7].

B. Satellite Optical Depth Retrieval

Radiative transfer theory provides the basis for methods used to characterize aerosol properties from satellite remote measurements. In a cloud-free, marine environment, the shortwave, solar radiation measured by a satellite radiometer is primarily the result of scattering by both molecular constituents of the atmosphere (Rayleigh scattering) and larger suspended aerosol (Mie scattering). Corrections to solar irradiance of less than 5% for ozone absorption are applied and aerosols are assumed to be non-absorbing. In the absence of sun glint, reflectance from the ocean surface is also small and contributions to the satellite-measured radiance due to surface foam and subsurface reflection are accounted for by empirical measurements.

For atmospheres with small optical depths such as the clear, marine atmosphere, contributions by multiple scattering can be neglected. After accounting for Rayleigh scatter, the satellite-measured radiance can be related to optical depth, as illustrated in Equation 6.

$$L_a = \frac{\omega_0 F_0}{4\mu} p(\psi_s)\delta_a \qquad (6)$$

where L_a is the measured radiance at the satellite due to aerosol scattering at a given wavelength, ω_o is the single scattering albedo, F_o is the incoming solar radiance at the top of the atmosphere, P is the scattering phase function, ψ_s is the scattering angle, δ_a is aerosol optical depth, and μ is the cosine of the satellite zenith angle [8].

Durkee, et al. [8] and Rouault and Durkee [9] proposed a method of parameterizing the scattering phase function, P, based on the ratio of the aerosol radiance measured in channel 1 (visible) and channel 2 (near-IR) of the NOAA AVHRR satellite sensor. Other recent multi-channel aerosol estimates have been presented by Veefkind, et al. [10]. Because the scattering efficiency of an aerosol distribution is wavelength dependent, scattering for a specific aerosol population peaks when the radius of the aerosol is nearly equal to the radiation wavelength. Subsequently, radiance counts measured by the AVHRR visible and near-IR channels will change with aerosol size distribution changes such that the ratio of channel radiances will be larger for smaller size particle distributions and smaller for larger size particle distributions. Durkee, et al. [8] called the ratio of the channel aerosol radiances the particle size parameter, S12. Since S12 varies pixel by pixel over the entire image, the scattering phase functions can be parameterized pixel-by-pixel allowing variations in aerosol distributions to be properly factored into the optical depth retrieval. In addition, the S12 permits characterization of the aerosol size properties for the clear air in the image.

1. Experiment

The satellite optical depth algorithm has been evaluated using from the 2-12 April 1996 EOPACE IOP, which was conducted off the Southern California coast. During this IOP the R/V Point Sur traversed the coastal zone with a vertical pointing 1.06 micrometer LIDAR (provided by TNO), frequent rawinsonde temperature and moisture measurements (provided by NPS) and surface layer aerosol measurements (published by University of Suderland). In addition, an instrumented aircraft measured aerosols and basic meteorological parameters in the region. Polar orbiting NOAA satellite data was received and processed at NPS for the period. This IOP was of particular interest in that significant changes in MABL properties and aerosols occurred during the measurement period.

2. Analysis Results

The R/V Point Sur moved southward along the coast on 3 April. During this day, low and mid tropospheric flow was from the northwest and maritime aerosols spectra dominated the MABL which was approximately 1100 m deep. NOAA satellite pass (not shown) from 2227 GMT 3 April showed clear conditions along the coast. The retrieved optical depth in this region was .25, which is associated with the larger-size marine aerosol size distribution and deep MABL. The S12 ratio for this area shows larger, maritime aerosols dominate the MABL. This is consistent with ship-based data and air trajectories for this day.

Significant changes occurred in the low-level flow during the next 24 hours. Strong offshore northeasterly flow developed. Doppler wind profilers in the region also show the development of a Santa Ana wind regime. The profiler at

the Ontario airport measured NE winds in excess of 30 knots during the afternoon of 4 April while the coastal profiler at Los Angeles (LAX) airport measured north and NE winds of 10-20 knots above 700 m.

Associated with this flow, an elevated layer of continental aerosols was observed by ship, aircraft and satellite sensors. An aircraft profile at 1853 GMT 4 April measured a distinct layer of aerosol extinction at 600-800 meters. Rawinsonde temperature, moisture, and wind data, collocated with the aircraft extinction data, are also included in this figure. These winds show NE winds in this layer of 15 to 20 knots. Lidar measured strong backscatter return in a layer from 400 to 700 m. The layer of strong backscatter is in agreement with the high extinction values from the aircraft.

The NOAA satellite data from 2216 GMT 4 April is presented in Figure 3. High values of optical depth are estimated over the entire Southern California coastal area. Values range from .17 to .38. There is a distinct plume of aerosols leaving the coast between Los Angeles and San Diego. The S12 ratio from this pass indicates a much higher ratio than 24 hours earlier, which indicates small aerosol sizes, typical of continental sources, are dominating the region. This is consistent with the lidar and aircraft data discussed earlier.

Figure 3
Optical depth estimates from NOAA AVHRR data for 2216 GMT 4 April 1996. The R/V Point Sur ship track is indicated by the solid line. Rawinsonde launch locations are denoted by dots.

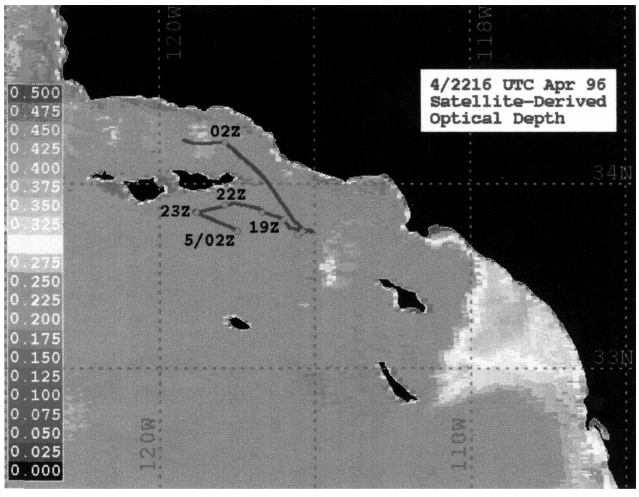

On April 5 the R/V Point Sur moved southeastward toward the plume observed by the NOAA satellite on 4 April. Subsidence associated with the offshore flow was quite intense this day and the MABL depths were very shallow, less than 100 m. Aircraft profiles and ship-based lidar continue to show aerosols in the lowest 1000 km. The aircraft data does not show a distinct layer of elevated extinction, but small values of aerosol extinction are present throughout the lowest 1 km. Satellite data for 2205 GMT 5 April (not shown) indicated lower values of optical depth (.15 to .25) but the remnant of the plume is still detectable.

The ship steamed though the plume location between 15 and 24 GMT 5 April. The stronger lidar backscatter values at that time are consistent with the satellite data. The S12 ratio continues to be high indicating smaller, continental aerosols over the coastal zone. In addition, Doppler wind profilers in the region also show the strengthening of this Santa Ana regime.

Northwest flow was re-established throughout the region by 8 April. The offshore flow ceased, the MABL deepened to 300 m, with NW low-level winds. This was accompanied by more low-level cloudiness in the MABL. In the clear areas, optical depth values decreased to .10 to .15 and the S12 ratio decreased indicating the return of maritime aerosols in the MABL. This was confirmed by in situ measurements aboard the R/V Point Sur.

A more complete discussion of the analysis results is available in Wash, et al. [11].

3. Optical Depth Study Conclusions

During this IOP satellite retrievals of aerosol optical depth and the ship and aircraft measurements were in good qualitative agreement. The NOAA satellite S12 ratio successfully depicted regions of maritime aerosol during the beginning and later parts of the IOP and the period of continental aerosol associated with the strong offshore flow of the Santa Ana event.

At this time, quantitative data from the lidar of aerosol extinction are not available. Therefore, a more quantitative assessment of satellite versus in situ data is not available. This will be a major priority in future studies with this and other IOP data sets.

The new generation of geostationary satellite, GOES-9, was operating over the West Coast at this time. The higher radiometric resolution from GOES-9 sensors provide the opportunity to retrieve aerosol depth. GOES-9 data from this period will be used to add to the temporal resolution of the satellite data for this period. In particular, GOES data should be able to monitor the development of the aerosol plume on 4 April.

Acknowledgments

This work was funded partially by the U. S. Office of Naval Research, program managers Dr. Scott Sandgathe and Dr. Ronald Ferek. A special thanks is due to Dr. D. R. Jensen for the SPAWAR Systems Center, San Diego, CA for his able organizational skills during EOPACE. The NPS work is supported by SPAWAR Systems Center, San Diego through Office of Naval Research funding. The Netherlands Minis-

try of Defense, assignment A95KM729, and the US Office of Naval Research, Grant N00014-96-1-0581, support the participation of TNO-FEL in EOPACE. Aerosol retrieval work at TNO-FEL is supported by SRON EO/008. Thanks to Carl Zeisse and Ike Bedall of SPAWAR Systems Center, San Diego, CA., for sharing optical propagation and their expertise. Thanks to Michael H. Smith and Martin K. Hill, Center for Marine Atmospheric Science, University of Suderland, United Kingdom for sharing aerosol data and their expertise.

Biographies

Kenneth Davidson and Carlyle Wash are Professors of Meteorology at the Naval Postgraduate School. Professor Wash is Chairman of the Department of Meteorology and Professor Davidson is Associate Chairman for research. They collaborate on research projects pertaining to assessment of atmospheric conditions that affect electromagnetic and Electro-optical propagation. Professor Davidson received a Ph.D. in Meteorology from the University of Michigan in 1970 and has been on the Naval Postgraduate School Faculty since. He served as an USAF weather officer prior to graduate studies at Michigan. His research investigations since 1966 has been on the structure of the atmospheric boundary layer; over land, water and ice with emphasis on air-sea and air-ice interaction and properties of the boundary layer relative to electromagnetic and optical wave propagation. Professor Wash received a Ph.D. in Meteorology from the University of Wisconsin in 1978 and has been on the Naval Postgraduate School Faculty since 1980. He served as in the Navy as Geophysics Officer prior to graduate studies at Wisconsin. His research and teaching interests have been in synoptic meteorology and satellite remote sensing.

References

1. Andreas, E. L., "Estimating C_n^2 Over Snow and Ice From Meteorological Data", *J. Opt. Soc. Am.*, 5A, 481-495, 1988.
2. Paulson, C. A., "The Mathematical Representation of Wind Speed and Temperature Profiles in the Unstable Atmospheric Surface Layer", *J. Appl. Meteorol.*, 9, 857-861, 1970.
3. Fairall, C. W., E. F. Bradley, D. P. Rogers, J. B. Edson and G. S. Young, "Bulk Parameterization of Air-Sea Fluxes for Tropical Ocean-Global Atmosphere Coupled-Ocean Atmosphere Response Experiment", *J. Geophys. Res.*, 101, 3747-3764, 1996.
4. Hill, R. J., "Implications of Monin-Obukhov Similarity Theory for Scalar Quantities", *J. Atmos. Sci.*, 46, 2236-2244, 1989.
5. Zeisse, C., S. Gathman, A. Barrios, B. Moision, K. Davidson, and P. Frederickson, "Low Altitude Infrared Transmission", *Proceedings, Battlespace Atmospherics Conference*, San Diego, CA, 2-4 December 1997.
6. Churnside, J. H., R. J. Lataitis and J. J. Wilson, "Two-color Correlation of Atmospheric Scintillation", *Appl. Optics*, 31, 4285-4290, 1992.
7. Frederdickson P. A., K. L. Davidson, C. Zeisse, and I. Bendall 1997. "Near-Surface Scintillation (C_n^2) Estimates from a Buoy Using Bulk Methods during EOPACE", *Proceedings, Battlespace Atmospheric Conference*, San Diego, CA, 2-4 December 1997.
8. Durkee, P. A., F. Pfeil, E. Frost, and R. Shema, 1991. "Global analysis of aerosol particle characteristics". *Atmos. Env.*, 25A, 2457-2471.
9. Rouault, M. and P. A. Durkee, 1992. "Characterization of aerosols from satellite remote sensing. In Nucleation and Atmospheric Aerosols", 357-360, N. Fukuta and P. E. Wagoner (Eds), A. Deepak Publishing
10. Veefkind, J. P., G. de Leeuw, and P. A. Durkee, 1997. "Satellite Remote Sensing of Aerosol Using ATSR-2 Data during TARFOX. American Geophysical Union Fall Meeting", December 1997, San Francisco, CA
11. Wash, C. H., M. S. Jordan, P.A. Durkee, P.A. Veefkind and G. de Leeuw, "EOPACE Satellite and In Situ Optical Depth Studies", *Proceedings, Battlespace Atmospheric Conference*, San Diego, CA, 2-4 December 1997.

Simulation of Drifters in a Turbulent Ocean

Roland W. Garwood, Jr., Ramsey R. Harcourt, and Rebecca E. Stone, Naval Postgraduate School, Monterey, CA

Introduction

Why do the proverbial flotsam and jetsam collect into streaks and patches at the surface of the ocean? The same Oceanic Planetary Boundary Layer (OPBL) forces that organize debris and plankton blooms at the ocean surface influence all freely drifting objects, including man-made platforms and buoys. Our interest in the answer to this question comes from a variety of environmental and defense-related needs. This includes prediction of phytoplankton blooms, oil spill management, mine warfare, search and rescue, and oceanographic sensing with Lagrangian drifters (Figure 1), to name a few. On a time scale less than an hour, near-surface convection of heat can alter or destroy a sound channel. Episodic seasonal convection initiates the global-scale thermohaline circulation, and it may modify the ocean-atmosphere climate on time scales from decades to centuries. Hence, advancement in the understanding and prediction of convection is important for predictions ranging from tactical sonar to climate and global change. In this brief article, we show computer predictions that illustrate how convection has special effects upon freely drifting material at all depths of the OPBL.

Large-Eddy Simulation of Convection

At the OPBL Laboratory of the Naval Postgraduate School, the opening question has been addressed with the specific purpose of understanding the motion and response of oceanographic sensor systems aboard instrumented floats. These floats have been released into the Labrador Sea as part of the Office of Naval Research Accelerated Initiative on Deep Oceanic Convection. The ultimate goal of this multi-institutional initiative is to learn to represent realistically turbulent processes and the thermodynamic consequences of convection in prediction models for ocean temperature, sa-

Figure 1

Schematic diagram of Lagrangian drifters [1] in LES-predicted OPBL turbulence. Drifters being carried by the convection have a one square meter cross sectional area and are not to scale. Such drifters are ideally suited for sensing the heat flux caused by the covariance between temperature and vertical velocity, <Tw>.

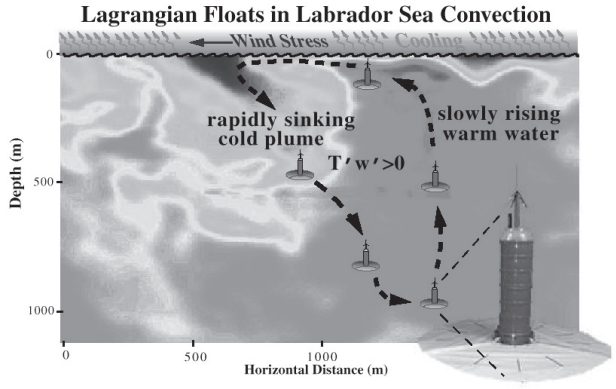

Figure 2

Surface temperature and Raleigh-Benard (R-B) circulation pattern associated with predominantly-free convection from a strong 400 w/ m² surface heat flux and light wind stress of 0.02 N/m² (caused by 3 m/sec winds). The horizontal scale of the largest R-B cells is similar to the depth (h) of the OPBL, which is 2 km in this case. The region shown is 6 km on each side.

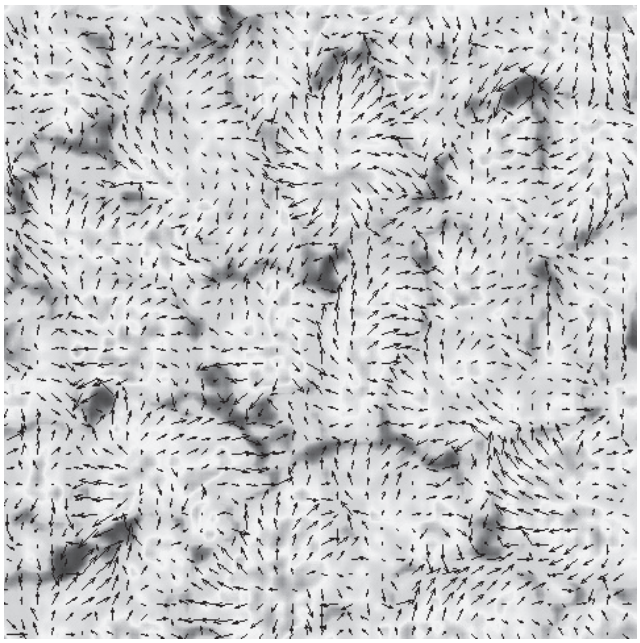

linity and velocity. In addition to traditional shipboard Eulerian oceanographic and atmospheric observations, Lagrangian and semi-Lagrangian observations are made by drifting packages of instruments.

Scientific interpretation of the observations of temperature and velocity from these drifters depends upon possible biases caused by the drifter motion. If a drifter behaves as a parcel of water and follows the water parcel trajectory, then it is purely Lagrangian. One of the drifter types used in the Labrador Sea was designed to be nearly Lagrangian [1]. If a drifter is designed to stay at a fixed depth but is free to be carried in any horizontal direction, then we term this drifter "isobaric." Two different drifter types with semi-Lagrangian isobaric designs were deployed in the Labrador Sea experiment. The RAFOS float [2] is fixed-depth, with passive ballasting. The profiling ALACE floats [3] have programmable ballasting, allowing both isobaric and profiling modes. Because all drifters are designed with either a passive or active ballasting mechanism, and a finite-sized drifter can only approximate the motion of a water parcel, no drifter is either purely Lagrangian or exactly isobaric. One objective of the OPBL Laboratory is to use computer simulation to demonstrate the consequences of different ballasting and drag designs. This leads to better understanding drifter behavior and possibly to optimize the sensor mix and deployment strategies to meet the observational goals.

Computer prediction of the time-dependent three-dimensional flow fields of the OPBL are provided by a Large-Eddy Simulation (LES) model [4,5,9]. Gridded temperature, salinity, velocity and pressure may be archived or used concurrently with the LES computations to predict motion of Lagrangian Drifter Models (LDM's) for the different drifter designs. Before showing the response of the LDM's, however, it is best to examine the variety of flow features that occur in the OPBL, in anticipation of the effects of organized turbulence structures upon drifting material.

LES results show that either free (Figure 2) or forced convection (Figure 3) may dominate, depending upon the magnitudes of surface heat flux, wind stress, and OPBL depth. Free convection predominates in the winter regimes of the subpolar and polar seas, especially in the very deeply convecting open water adjacent to marginal ice zones. In Figure 2, the wind stress is relatively light, so the buoyancy-driven Raleigh-Benard (R-B) cells tend to be radially symmetrical. These R-B cells consist of warmer water that rises from depth to the surface. This water is displaced upward by the rapidly descending plumes of surface-cooled water that originate in the cooler and more dense water between the R-B cells. Energy to drive the sinking plumes, and in turn the R-B circulation, is derived from the buoyancy flux associated with the release of heat and radiation to the atmosphere. The speed of the descending plumes (w) may be several cm/sec. The approximate diameter of the R-B cells scales with the depth (h) of the OPBL, which may vary from 10's of meters to more than a kilometer. As the OPBL deepens due to the accumulated effects of storm mixing and seasonal cooling, the vertical overturning time scale (h/w) of the free convection increases to become comparable to the inertial period (order 1 day). Then Coriolis force increasingly causes the R-B cells

Figure 3
Same as for Figure 2, except with a strong wind stress in the y-direction of 1.0 N/ m2 (caused by 20 m/sec winds). Horizontal rolls cause very strong convergence lines that lie about 45 degrees to the right of the wind.

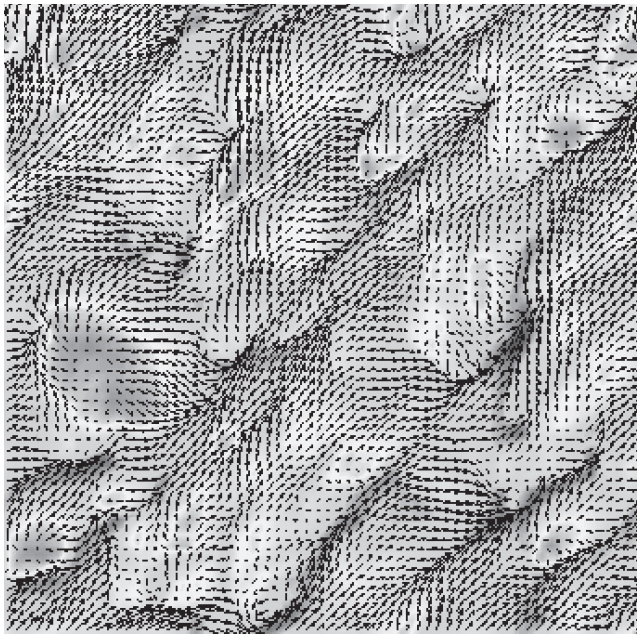

to rotate clockwise (northern hemisphere), as the flow diverges horizontally. This rotation and the natural unsteadiness of the turbulence prevent the R-B cells from assuming the classical hexagonal pattern of steady-state nonrotating free convection. Any drifting bodies and material floating on the surface will tend to be collected in the convergence zones between the R-B cells.

Forced convection is more important during the autumn storm forcing of temperate and subpolar seas, with mixing driven by kinetic energy from the wind. In Figure 3, a strong wind stress accompanies the surface cooling and sets up a circulation having extended convergence lines that lie in a direction approximately 45 degrees to the right of the wind stress direction. Because of the Coriolis force, these convergence lines are the surface manifestation of sets of horizontal rolls with opposing rotational directions. R-B cells are still evident, but freely drifting material at the surface will tend to collect in convergence zones produced by the wind-driven circulation. Most commonly, forced convection and free convection occur together. In the polar seas, forced convection may be an important precursor to free convection. The organized rolls of forced convection may help dilate a frazil ice field to create leads and enhance heat and buoyancy exchange between the OPBL and the atmosphere, helping to perpetuate deep convection [6].

Yet another kind of organized cell structure is possible in the coldest and deepest oceanic convection - thermobaric conditional instabilities [7,4]. The term “thermobaric” refers to the nonlinear density effect of temperature and pressure together to increase the downward acceleration of sinking plumes of cold water. In normal convection, water parcels do not escape the OPBL. Rather, the turbulent OPBL deepens as it entrains the underlying nonturbulent stratified water. However, the unusual thermobaric plumes of the polar-sea OPBL may be detrained - escaping the OPBL much as cumulus clouds escape the atmospheric planetary boundary layer. Figure 4 shows an LES prediction of the onset of a field of thermobaric conditional instabilities in the Greenland Sea [8]. In Figure 5, a single plume extends 400 m into the otherwise stable and nonturbulent layers beneath a 200-m deep OPBL. With mass escaping the OPBL, the depth of the OPBL may decrease - in opposition to the tendency of the OPBL depth to increase by entrainment. Lagrangian drifters

Figure 4
A temperature isosurface marks the lower boundary of a 200-m deep OPBL in this 3-D picture, with the horizontal dimensions being 1.5 km on a side. A number of thermobarically unstable plumes extend below the OPBL by 50 m to 150 m.

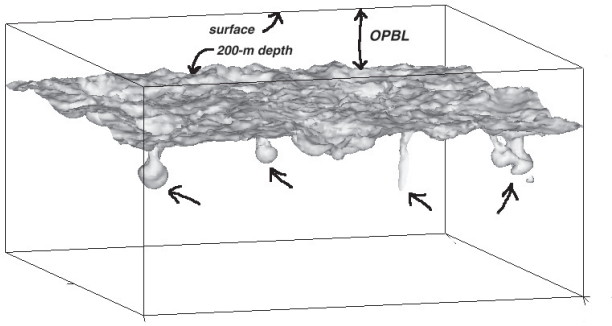

Figure 5
An x-z slice of the temperature field from the same simulation as for Figure 4, showing a single thermobaric plume that penetrates 400 m into the underlying stable water mass. Scales are in meters. The coldest water (shaded darkest) is colder than -1.1 C. The warmest water (white) is warmer than -0.4 C. In the polar seas, warmer water underlies colder water because salinity dominates the density (low salinity in the OPBL and higher salinities below 200 m).

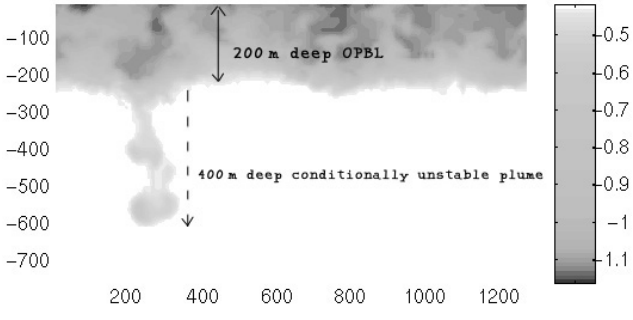

and particulate matter trapped in such conditionally unstable plumes may be carried downward below the OPBL with speeds of possibly hundreds of m/hr - perhaps the highest vertical ocean current velocities on earth. As a corollary, drifters residing in the underlying stable water being penetrated by the conditionally unstable plumes will rise slowly because of water mass conservation.

Simulation of Drifters in a Convective Ocean

With pre-computed LES velocity, pressure, temperature and salinity fields, Lagrangian and isobaric drifter motion and sensor response may be predicted iteratively, Figures 6 and 7 respectively. The turbulent kinetic energy (TKE) and turbulent fluxes of heat, mass and momentum detected by these LDM's are evaluated and compared with the Eulerian calculations (gridded data) from the numerical experiments. The numerical results indicate that Lagrangian drifters can potentially resolve well the TKE, the heat flux, as well as nutrient and other tracer fluxes. Lagrangian drifters are also able to define the time-dependent vertical and horizontal scales of the convecting plumes. Observations of velocity and temperature by purely Lagrangian drifters will not be biased. However, actual drifters will not always perform ideally, and realistic LDM's for these drifters are being constructed which will assist in the analysis of the field data provided by these drifters. In Figure 6, one of the idealized and unbiased Lagrangian drifters was temporarily detrained from the OPBL and later re-entrained. This may not happen with real LDM's that will have a small positive buoyancy when in the lower reaches of the OPBL.

Figure 6
An ensemble of time-dependent depth records for Lagrangian drifters in the 28-day prediction of the 1997 wintertime convection of the Labrador Sea. The dashed line is an analysis of the OPBL depth for the period. These purely Lagrangian drifters repeatedly circulate from the surface to the bottom of the OPBL.

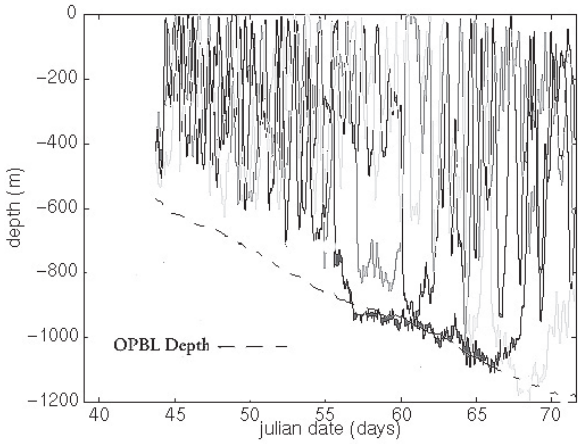

Compared with the Lagrangian drifters, the isobaric drifters' sampling statistics are biased. The isobaric drifters will sense mean fields for temperature and velocity that will be biased by the tendency for the fixed-depth drifters to seek out and maintain position in zones of horizontal convergence. Depending upon the ballasting depth, these drifters will experience a significant mean vertical velocity that is caused by the turbulence, not by a true mean upwelling/downwelling. The vertical current may be either up or down. If located in the upper reaches of the OPBL, the isobaric drifters will experience a downward flow. Drifters in the lower regions of the OPBL will experience an upward flow. As Figure 7 shows, the 95-m drifter most near the surface encounters a strong downward mean velocity of more than 1 cm/sec, resulting in an apparent vertical displacement of 25 km during the February-March 1997 period of simulated Labrador Sea convection. The drifter at 237 m experiences an upwelling before about day 60, and then a downwelling, after the OPBL deepened below 1 km. The 712-m drifter has little vertical flow until after it is entrained into the deepening OPBL on day 62. Thereafter it experiences an upward flow of nearly 1 cm/sec. From these results, we conclude that isobaric drifters should be particularly likely to observe the most significant plumes and largest vertical velocities. Experimentally, a combination of Lagrangian and isobaric drifters may be best to both measure accurately the fluxes and track convection.

In closing, insight into optimal drifter sampling strate-

Figure 7
The time-integrated vertical velocity of four isobaric drifters, simulated for the same period as for Figure 6.

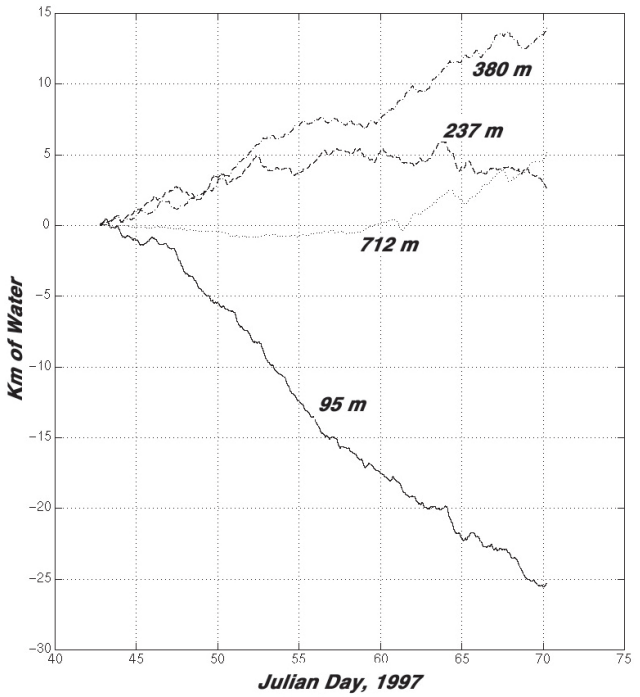

gies might be gained by considering the behavior of marine organisms. Do plankton and higher marine organisms use convection to enhance survivability? Tracers or neutrally buoyant and passive organisms will be advected like Lagrangian drifters, with effective diffusion and dispersion rates well simulated by the Lagrangian drifter results here. However, like the isobaric drifters in Figure 7, organisms that maintain a particular depth in the upper third of the OPBL, either by ballasting or by swimming, will statistically experience a large mean downwelling. Similar isobaric organisms in the lower two-thirds of the layer may experience a large upwelling. By maintaining a nearly fixed depth, such organisms should experience a continual vertical current with flow speeds as large as hundreds of meters per day, depending upon the surface forcing. Other organisms may "ride" the vertical currents as pure Lagrangian drifters, possibly extending their vertical range advantageously. These simulations provide some new insight into the response of typical drifters to convective oceanic flow fields, and they are a basis for future simulation of turbulent advection of drifters - both man-made and natural.

Acknowledgments

This research was supported by the Office of Naval Research (Code 322OM) and by the National Science Foundation (DPP-9114161). LES computations were accomplished with a grant of HPC time from the DOD HPC Center. This support is gratefully acknowledged.

Biographies

Roland Garwood received a BS in Electrical Engineering from Bucknell University in 1967. He received a Ph.D. in Oceanography from the University of Washington in 1976, after serving as a NOAA commissioned officer from 1968-71. He joined the faculty of the Naval Postgraduate school's Department of Oceanography in 1976, specializing in ocean dynamics and air-sea interactions.

Ramsey Harcourt is a research assistant in the Department of Oceanography at the Naval Postgraduate School. He received a Masters in Physics from the University of California at Santa Cruz in 1991. His primary interest is Large Eddy Simulation of the ocean turbulent boundary layer, and he is currently writing a Ph.D. dissertation on the behavior of drifters in open ocean deep convection.

Lieutenant Commander Stone was commissioned in the U.S. Navy in 1985; after a shipboard tour, she became a Navy Oceanographer, serving in Washington, D.C. and in Guam. She received Masters degrees in both Meteorology and Physical Oceanography from the Naval Postgraduate School, where she is a doctoral candidate.

References

1. D'Asaro, E. A., A Lagrangian float, J. Atmos. Oceanic Technol., 13, 1230-1246, 1996.
2. Rossby, T., D. Dorson, and J. Fontaine, The RAFOS system, J. Atmos. Oceanic Technol., 3, 672-679, 1986.
3. Davis, R. E., D. C. Webb, L. A. Regier, and J. Dufour, The autonomous Lagrangian circulation explorer (ALACE), J. Atmos. Oceanic Technol., 9, 264-285, 1992.
4. Garwood, R. W., Jr., S. M. Isakari and P. C. Gallacher, Thermobaric convection, in The Role of the Polar Oceans in Shaping the Global Environment, Ed. by O. Johannessen, R. Muench and J. Overland, Am. Geophys. Union Monograph, Vol. 85, 199-209.
5. Harcourt, R. R., L. Jiang, and R. W. Garwood, Jr., Numerical simulation of drifter response to Labrador Sea convection, Tech. Rep. NPS-OC-98-001, Naval Postgraduate School, Monterey, 71 pp., 1998.
6. Carsey, F. D. and R. W. Garwood, Jr., Identification of modeled ocean plumes in Greenland Gyre ERS-1 SAR data, Geophys. Res. Lett., 20, 2207-2210, 1993.
7. Garwood, R. W., Jr., Enhancements to deep turbulent entrainment, In Deep Convection and Deep Water Formation in the Oceans, Ed. by P. C. Chu and J. C. Gascard, 197-213, 1991.
8. Stone, R. E., Deep mixed layer entrainment, MS thesis, Naval Postgraduate School, Monterey, 67 pp., March 1997.
9. http://www.oc.nps.navy.mil/opbl is the OPBL Laboratory home page.

Megaripples in the Nearshore

Edward B. Thornton, Edith L. Gallagher, and Timothy P. Stanton, Oceanography Department, Naval Postgraduate School, Monterey, CA

Introduction

Megaripples, nearshore bedforms with heights up to 50 cm and lengths of 1-10 m, are ubiquitous in nature, but only recently has their widespread occurrence been recognized. Megaripples significantly affect sand transport in two ways, through increased suspension of sediment and by migration of the ripples themselves (i.e., volume transport). In addition, they act as hydraulic roughness elements, changing wave dissipation and water circulation patterns. However, because their importance has only recently been realized, there are few observations of megaripples and they are poorly understood. As a result, most models for predicting wave dissipation, current generation, sediment transport, and beach change assume that the sand bed is smooth and uniform, but this is a significant oversimplification, as the seafloor inside the surf zone is bumpy and irregular.

Background

The sand bed on a beach is composed of complex bedforms caused by varying wave and current regimes (Allen, 1968, Clifton, et al., 1971). With the exception of small wave ripples outside the surf zone, few quantitative observations of bedforms in the nearshore are available, and the first simultaneous wave and current measurements have only recently been made (Hay and Wilson, 1994). This lack of data is due to difficulties in making measurements in the harsh nearshore environment. *In situ* observations historically have been made by divers who are limited by visibility and rough conditions, such that observations are impossible even in the mildest of storms. Internal sedimentary structures (e.g., layering in sandstones) also are used to study bedforms in the nearshore. Evidence of beforms is seen in the structures beneath the sand surface and assumed to be related to the

configuration of bedforms when the layers were laid down. However, if the beach is eroding these structures are destroyed. Clifton, et al. (1971) studied the cross-shore variation of bedforms (using both divers and sedimentary structures) on a near-planar beach. Davis and Fox (1972), Davidson-Arnott and Greenwood (1976), and Hunter, et al. (1979) similarly examined barred beaches. The dominant bedforms just seaward of the breaking waves were found to be lunate megaripples pointing in the direction of wave propagation, which were attributed to asymmetric wave velocities under shoaling waves. Progressing shoreward, the sand bed often was observed to be flat under breaking waves owing to breaking-induced turbulence and high wave velocities, which causes sheet flow conditions (a thick moving layer of sand which planes the bed). Inside the surf zone, the seafloor was observed to be complicated by the occurrence of bed features driven by unidirectional flows (rips, tidal currents, and longshore currents) as well as asymmetric waves.

Based on these observations and crude measures of the fluid velocity, Clifton (1976) developed an empirical model for bedform regimes in the nearshore, similar to steady flow bedform regime models for rivers and channels. He suggested that small-scale morphology under waves increases from small wave ripples to cross-ripples to megaripples with increasing stress until a critical stress is achieved and the bed is planed-off during sheet flow conditions. However, since the beach is generally eroding (destroying sedimentary sequences) during storms and detailed field observations in the surf zone for high energy conditions have not been available, the model has not been verified for large waves and currents. Owing to this lack of information on bedforms in the nearshore, most circulation and sediment transport studies assume that the bed is smooth and uniform, and that the parameter accounting for the bottom roughness, the bed shear stress coefficient C_f, is constant. Motivation for our work is based on the need to quantitatively determine the influence of small-scale morphology on nearshore sediment transport and hydrodynamics in all weather conditions, especially during storms when the most dramatic changes in the beach take place.

Recently, acoustic means have been used to measure bedforms inside the surf zone, and measurements have been possible during more energetic conditions. Ripples were measured using a fixed array of three acoustic altimeters plus a fourth in side-scan mode by Vincent and Osborne (1993). Both small (height 2 cm) and medium (height 8 cm) ripples were observed to coexist outside the surf zone, but the small ripples were destroyed by plunging breakers inside the surf zone. Hay and Wilson (1994) measured bedform plan views on the crest of a nearshore bar using a rotary side-scan sonar. The images showed rapid changes in ripple types during the waning stages of a storm, on time scales of 1-3 hours. These techniques were considered to be quite promising and have been developed further.

Recent Work

For the last decade, the North American nearshore research community has focused their energy on conducting a series of comprehensive field experiments over the barred beach at Duck, N.C. (SuperDuck,1986; DELILAH, 1990; Duck94, 1994; SandyDuck, 1997). Duck was chosen as the field site because of the logistical support provided by the U.S. Army Field Research Facility located there, and in particular the availability of the unique, 12 m-high, three-wheeled, motorized, amphibious surveying vehicle called the CRAB (Figure 1). This remarkable vehicle solved the problem of obtaining accurate bathymetry over large areas in almost all weather conditions and also provides a stable platform for the deployment of sensors and making measurements.

The Duck94 nearshore field experiment (a pilot study to the SandyDuck experiment discussed below) represented a first attempt to make quantitative, multi-scale measurements of nearshore morphology. During Duck94, daily surveys of a .5 x .5 km area (Figure 2a) were made with the CRAB and small-scale morphology was measured using a variety of techniques. We measured seafloor height variations using a single 1 MHz automatic gain control (AGC) sonar altimeter (Gallagher, et al., 1996) and a 500 kHz side-

Figure 1
CRAB (Coastal Research Amphibious Buggy). The CRAB is about 12 m tall, 8 m wide at the rear wheels (forward is toward the left), and the diameter of the tires is about 1.7 m. It is shown during the SandyDuck nearshore field experiment with an array of altimeters (on pipes hanging from the rear cross beam) and a side scan sonar (just behind the front wheel, also mounted below the main cross beams of the CRAB, about 0.8 cm above the bed).

scan sonar mounted on the CRAB (Thornton, et al., 1998). We also mounted AGC altimeters on stationary frames located throughout the surf zone (Gallagher, et al., 1998) including a small two-dimensional array (1.5 x 1.5 m) of altimeters in the trough (at cross-shore position x=170 m and longshore position y=940 m in Figure 2a) to measure bedform migration (Gallagher, et al., accepted). In addition, rotating side-scan sonars were deployed at three locations across the surf zone (Hay and Bowen, in press).

Thornton, et al. (1998) found significant variations both temporally and spatially in the small-scale bathymetry measured with both the altimeter (Figure 2b-e) and the side-scan sonar (Figure 3) mounted on the CRAB. Three cases were examined in detail and Clifton's (1976) model was found to both compare and contrast with observed bedforms in the nearshore. This suggests that the model may not be sufficient for all beaches and all conditions. Further analysis indicated that newly formed ripples coexisted with residual ripples from the past to form complex, multi-scaled ripple patterns.

Garcez Faria, et al. (1998) determined values for the bed shear stress coefficient C_f (generally taken to be constant) from vertical velocity profiles and found that C_f values varied by an order of magnitude across the surf zone. So much variability was a surprise, but perhaps not so surprising was the observation that C_f values were correlated with bottom roughness (r=0.8, see their Figure 14) estimated with the single altimeter on the CRAB. This result suggests that increased bed shear stress is due to enhanced form drag of the bedforms and that to predict realistically nearshore currents, a spatially variable C_f is needed. Unfortunately, predictions of spatially varying bed roughness and C_f do not exist.

Using the stationary array of sonar altimeters in the trough, significant temporal variations (Figure 4a) in the small-scale morphology were observed and bedforms in the trough migrated at rates of 10-170 cm/hr (Figure 4b). Gallagher, et al. (accepted) showed that megaripples did not fall into any traditional class of bedforms: with crests oriented transverse, longitudinal, or oblique to the resultant vector. However, the direction of megaripple migration was such that gross sediment transport normal to the bedform

Figure 2

a) Large-scale bathymetry measured by the CRAB during Duck94 (20 Oct 1994). The sticks show the fixed instrument locations and the thick line shows the area represented in Figure 3. b-e) Elevation of the seafloor below mean sea level versus cross-shore position (at longshore position y=930 m in Figure 2a) as measured by the CRAB (dashed line, offset by -50 cm) and small-scale morphology measured with a single sonar altimeter mounted on the CRAB (solid line) during Duck94. b) Oct 8, c) Oct 10, d) Oct 11, e) Oct 12.

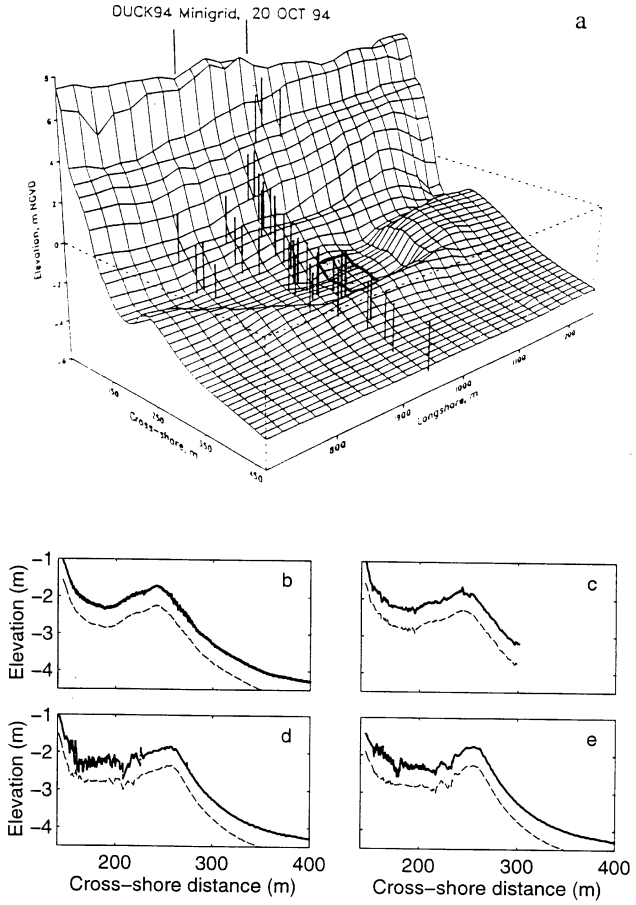

Figure 3

Side-scan sonar image (from area denoted by the heavy line in Figure 2a) showing megaripples in the throat of a rip current-generated hole in the bar (Figure 2a). (Onshore is toward the top of the figure and North is to the right.)

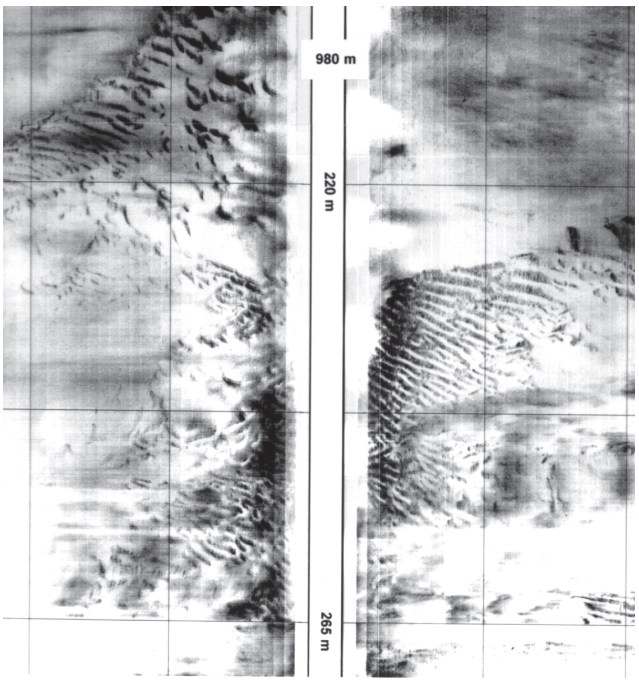

Figure 4
a) Distance to the seafloor below a single sonar altimeter located in the trough of a barred beach for 2 months during Duck94 versus time. b) Distance to the seafloor (26-27 Sep 1994) below closely spaced sonar altimeters in the trough versus time. The altimeters are separated in the cross-shore by 80 (upper to middle panel) and 60 cm (middle to lower panel). Time series in the top panel is from the most onshore altimeter. Lines connecting 'troughs' of bedforms illustrate onshore migration of the features (about 30 cm/hr).

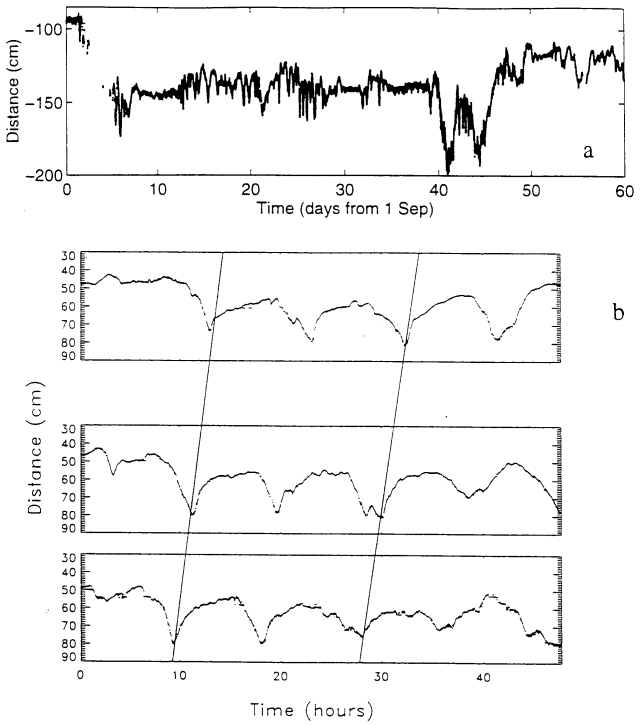

crest was maximized, similar to the theory for alignment of subaerial dunes by Rubin and Hunter (1987). The implication of this finding for modelling sediment transport and beach erosion and accretion is significant; it says that the intuitive flow direction (i.e., the resultant fluid vector direction) predicts poorly the direction of migration of the features and therefore any transport associated with the bedforms.

Continuing Work

The SandyDuck experiment, which took place in Sep-Oct 1997, was the last in the series of large collaborative experiments at Duck, NC. Included were many scientists, outstanding logistic support, hundreds of instruments (>130 wave and >55 velocity sensors) and the most comprehensive measurements of the surf zone ever made. A complete description of the experiment can be found at http://www.frf.usace.army.mil/SandyDuck/SandyDuck.html.

Our successes during Duck94 led to further development and improvement of our instrumentation for SandyDuck. Small-scale morphology measurements were improved by replacing the single altimeter mounted on the CRAB during Duck94 with an array of seven altimeters (Figure 5) and upgrading the side-scan sonar to record digitally (in collaboration with Prof. Tom Drake, NCSU). The altimeter data is being converted into "maps" of bedforms over the daily survey area to give a quantitative, 3-D measure of the spatial distribution of bedforms, their characteristics (wave length, height, etc.) and their relation to the large scale bathymetry within the nearshore (out to depths of 6 m). These parameters can be corroborated using the side-scan. Bottom shear stress was also measured from a movable sled (that crossed the surf zone once per day, stopping for hour-long measurements) and these data are being used to expand the study of Garcez Faria, et al. (1998).

Preliminary results from this experiment suggest the spatial and temporal variability is more complicated than we had imagined. Figure 6a shows seven cross-shore profiles of small-scale bathymetry from the shoreline (at x=130 m) to outside the surf zone (x=400 m) as measured by the array of sonars on the CRAB. Large (30 cm), irregular bedforms are seen inside the surf zone (x=150 - 205 m, expanded in Figure 6b) extending to the crest of the bar. On parallel profiles only 50 meters away (Figure 6c), very different bedforms are seen, also extending across the surf zone, but much smaller in amplitude and wavelength. These observations suggest, as did Thornton, et al.'s (1998), that a simple 1-D model like Clifton's (1976) may not be sufficient to describe the complex seafloor in the nearshore. Megaripples, like those seen in Figure 6b, always occurred in at least part of the daily .5 x.5 km survey area, and their distribution has been difficult to predict using standard observational tools (i.e., high vs low tide, big vs small waves, strong vs. no currents, presence or absence of rips currents, etc.). Further analysis of these data, as well as the side-scan sonar data and

Figure 5
A close-up of the sonar array mounted on the rear axle of the CRAB. Each altimeter hangs on a rigid 1.5 m-long pipe with the transducers nominally 0.7 m from the sand bed.

Figure 6

a) Elevation of the seafloor below mean sea level (profile marked with asterisk) versus cross-shore position as measured by an array of sonar altimeters mounted on the CRAB (Figure 1). The unmarked profiles are offset from the profile marked with an asterisk to represent the horizontal separation of the sensors in the lagged array (from top to bottom, lags=180, 150, 60, 15, 30, 90 cm). b) Expanded view of trough area for four altimeter profile lines (separations between sensors, from top to bottom, are 90, 15, and 60 cm). c) Expanded view of trough area for four altimeter profile lines (the same four sensors as in panel b) approximately 20 minutes earlier and 50 m to the south. Data gaps occur when altimeters are not submerged.

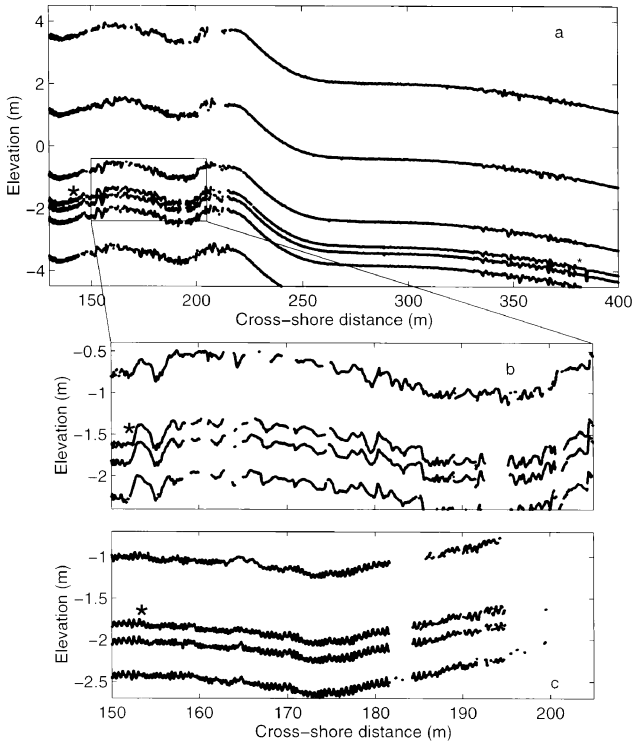

sedimentological data, will help to elucidate the complexity of the seafloor in the nearshore.

In addition, similar measurements are being planned for fall 1998 and 1999 as part of the European Commision-funded MAST program's COAST 3D experiment series (a full description may be found at www.frw.ruu.nl/fg/wesp.html). Using the new Dutch version of the CRAB detailed measurements, like those obtained at Duck, will be obtained for very different beaches in the Netherlands and England.

Conclusion

Recent observations suggest that megaripples, irregular bumps and holes, are ubiquitous in the surf zone. However, because their importance has only recently been realized, they are poorly understood. Our ongoing studies involve the measurement and analysis of small-scale morphology in the surf zone. Our working scientific hypotheses are 1) that bedforms in the nearshore are an important mechanism for sediment transport, 2) that they increase dissipation of waves and currents via form drag and are therefore important to understanding fluid dynamics, and 3) the processes which form them are similar those in rivers and deserts, so that existing models may be applicable. Both existing and newly acquired data sets are being used to investigate these hypotheses.

Biographies

Distinguished Professor Thornton received his Ph.D. from the U. of Florida in Ocean Engineering in 1969 and has been a Professor of Oceanography at the Naval Postgraduate School since 1969. He has been a principle investigator and on the planning committees of all the comprehensive nearshore experiments in the U.S. over the last two decades. He has been funded by ONR since 1972 in the study of nearshore wave processes and has more than 50 scholarly publications.

Edith Gallagher is a National Research Council postdoctoral associate at the Naval Postgraduate School working with Prof. Thornton. She received her Ph.D. in oceanography from Scripps Institution of Oceanography in 1996. She studies sand transport, erosion and accretion, and beach change using innovative modelling techniques and unique measurements from natural beaches.

Associate Research Professor Tim Stanton has been in the oceanography department at the Naval Postgraduate School since 1978 after receiving a M.S. in physics from the University of Auckland, New Zealand. He has been principle investigator on nine ONR, and NSF research programs studying oceanic turbulent boundary layers and waves in the open ocean, coastal margin and Polar regions. He has developed a range of instrument systems for measuring dissipation and stresses in the ocean, including the first field deployed cm-scale three component acoustic doppler current sensors.

REFERENCES

Allen, J.R.L. (1968) *Current Ripples: their relation to patterns of water and sediment motion.* North Holland, Amsterdam, pp 433.

Clifton, H.E., R.E. Hunter and R.L. Phillips (1971) Depositional structures and processes in the non-barred high-energy nearshore. *J. of Sedimentary Petrology*, 41 (3), 651-670.

Clifton, H.E. (1976) Wave-formed sedimentary structures-A conceptual model. In Davis and Ethington ed: *Beach and Nearshore Sedimentation, SEPM Special Publication*, 24, 126-148.

Davidson-Arnott, R.G.D. and B. Greenwood (1976) Facies relationships on a barred coast, Kouchibouguac Bay, New Brunswick, Canada. In Davis and Ethington ed: *Beach and Nearshore Sedimentation, SEPM Special Publication*, 24, 149-168.

Davis, R.A. and W.T. Fox (1972) Coastal processes and nearshore sand bars. *J. Sedimentary Petrology*, 42, 401-412.

Gallagher, E.L., W. Boyd, S. Elgar, R.T. Guza and B. Woodward (1996) Performance of a sonar altimeter in the nearshore. *Marine Geology*, 133, 241-248.

Gallagher, E.L., S. Elgar and R.T. Guza (1998) Observations of sand bar evolution on a natural beach. *J. Geophysical Research*, 103, 3203-3215.

Gallagher, E.L., S. Elgar and E.B. Thornton (1998) Observations and prediction of megaripple migration in a natural surf zone. *Nature* (accepted).

Garcez Faria, A.F., E.B. Thornton, T.P. Stanton, C.V. Soares and T.C. Lippmann (1997) Vertical profiles of longshore currents and related bed shear stress and bottom roughness. *J. Geophysical Research*, 103, 3217-3232.

Hay, A.E. and A.J. Bowen (1998) Alongshore migration of lunate megaripples during DUCK94. *J. Geophysical Research* (in press).

Hay, A.E. and D.J. Wilson (1994) Rotary sidescan images of nearshore bedform evolution during a storm. *Marine Geology*, 119, 57-65.

Hunter, R.E., H.E. Clifton and R.L. Phillips (1979) Depositional processes, sedimentary structures, and predicted vertical sequences in barred nearshore systems, Southern Oregon Coast. *J. of Sedimentary Petrology*, 49(3), 711-726.

Rubin, D.M. and R.E. Hunter (1987) Bedform alignment in directionally varying flows. *Science*, 237, 276-278.

Thornton, E.B., J.L. Swayne and J.R. Dingler (1998) Small-scale morphology related to waves and currents across the surf zone. *Marine Geology*, 145(3-4), 173-196.

Vincent, C.E. and P.D. Osborne (1993) Bedform dimensions and migration rates under shoaling and breaking waves. *Continental Shelf Research*, 13(11), 1267-1280.

Profile in Science

Edward B. Thornton

Dr. Edward B. Thornton is Professor of Oceanography at the Naval Postgraduate School, Monterey, California. After graduating with a PhD in Coastal and Oceanographic Engineering in 1969 from the University of Florida, Professor Thornton joined the faculty of the Postgraduate School. He teaches courses in nearshore oceanography, wave theory, and signal processing. Since 1972, the Office of Naval Research has funded Professor Thornton in the study of nearshore wave processes. In 1996, he was accorded the title of Distinguished Professor at the Postgraduate School. He is a member of American Geophysical Union, American Shore and Beach, Sigma Xi, and American Society of Civil Engineering for which he served on several technical subcommittees. He served also on the National Research Council Committee on Coastal Engineering Measurement Techniques. In 1991, he received the Minna-Heineman-Stiftung Environmental Scientist Award from the Technical University of B raunschweig, Germany , and the Hydrographic Institute of Portugal Medal in 1991. He has written more than 50 scholarly publications.

Subsurface Lagrangian Measurements in the Northeastern Pacific Ocean

Curtis Collins, Newell Garfield, Robert Paquette, and Thomas Rago, Department of Oceanography, Naval Postgraduate School, Monterey, CA
Everett Carter, Taygeta Scientific Inc, Monterey, CA

Introduction

In 1992, we began a Lagrangian study of intermediate depth (150 – 600 m) flow of waters off the Central Coast of California. One goal of our program was to measure the path and continuity of the poleward flow adjacent to the coast. The poleward flow carries warm, salty water from equatorial regions and is called the California Inshore Current (or the Davidson Current) in winter and the California Undercurrent during the rest of the year. Floats should also determine how these equatorially derived waters intertwine and mix with the cool, fresh subarctic waters which are found offshore. The primary offshore exchange of surface waters appears to take place through the offshore flowing filaments that appear to be anchored to major capes along the California Coast. We planned to investigate whether this same pattern occurred at intermediate depths or whether the mixing of heat and salt from the poleward flow was a process occurring continually along its path.

We used isobaric RAFOS floats for these studies (Rossby, et al., 1986). The RAFOS system requires both floats and sound generating sources. The sources are moored at fixed locations and generate 80 s chirps twice a day. The floats are free floating hydrophones, which record the time of arrival of the source broadcasts along with in situ pressure and temperature. This system provides the ability to tag and track subsurface flow for long distances and long time periods at reasonable cost. In the Northeastern Pacific, the axis of the sound channel is relatively shallow (500 - 700 m), facilitating the study of intermediate level flow. Further, the availability of the SOSUS arrays along the West Coast allows monitoring of the timing and strength of our sources.

Results for the California Current System

The view of the California Current system yielded by these floats is markedly different than that given by surface drifters (Brink, et al., 1991) or dynamic topography (Lynn and Simpson, 1987). The floats (Figure 1) clearly show poleward flow next to the coast, an absence of equatorward flow offshore, and a variety of eddy motions propagating westward. While some of the characteristics of the eddies are similar to those seen by the surface drifters, the subsurface floats show a predominance of smaller scale motions. Below we briefly discuss each of these features.

Most of the floats were launched over the continental margin in the region between San Francisco Bay and Monterey Bay. The length of time each float remained submerged varied depending on the specific objectives of each float deployment. At the end of the specified submerged period, the float released a ballast weight and surfaced in order to relay its stored data via a satellite link. While the floats are considered expendable, four have been recovered, two off Oregon, one off southern California, and one at Hawaii. Two others went ashore along the Southeastern Alaska coast but have not been recovered.

Six of our floats were entrained into the poleward flow along the coast for periods between one and two months. The floats were carried a mean alongshore distance of 390 km. The coherence of this flow between Pt Reyes and Cape Mendocino was strong (Collins, et al., 1996). At Cape Mendocino, one of the floats was caught in an offshore flowing filament, but the others continued north to Cape Blanco. Near Cape Blanco, the floats appear to leave the continental margin, moving offshore into Cascadia Basin where they become entrained in anticyclonic eddies. The floats confirmed the presence and continuity of the poleward flow and demonstrated that this flow is not strongly influenced by the offshore flow of surface waters at capes. The floats also reveal the vertical structure of the poleward flow: strongest flow occurred between 100 and 150 m and diminished with depth to at least 900 m. Other data suggest that the poleward flow extends even deeper.

Figure 1
Trajectories for intermediate (150-600 m) depth RAFOS released off Central California during the period 1992-1995. The "o" indicates the launch point and "x" the point where the mission ended (Garfield et al., 1998). Oceanographers call this figure a "spagetti diagram." A movie of the trajectories can be viewed at http://www.oc.nps.navy.mil/~garfield/.

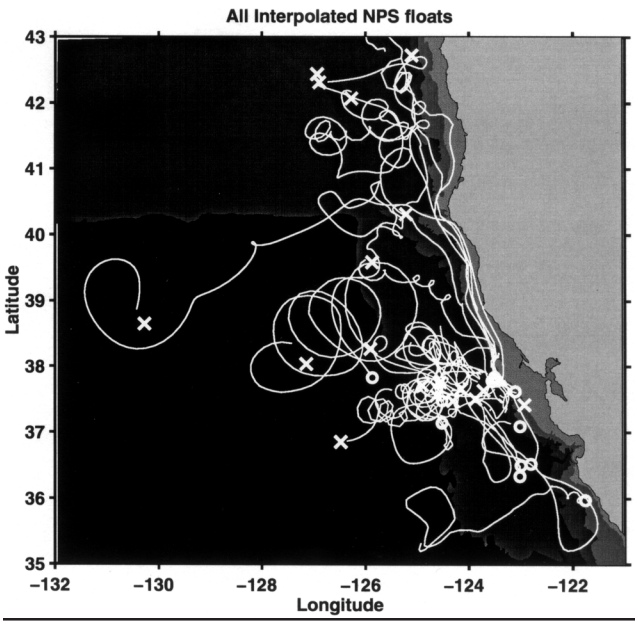

Almost all the floats, those transported poleward and those that moved westward soon after deployment, encountered eddy motion as they entered the ocean interior. The large number of observed eddies confirms that the circulation at intermediate depths in the ocean is characterized by an energetic eddy field. Like most other regions where Lagrangian studies have occurred, the deep ocean circulation is neither quiescent nor composed of a steady mean flow. Eddies are continually present and provide an important mechanism for transporting water long distances into the ocean interior. For coastal waters off California, eddies appear to play the major role in terms of the onshore-offshore transport of intermediate level waters.

In the ocean interior, three patterns of eddy motion were seen, although two of the patterns were each observed by only single floats. The float that was caught up in the offshore flowing filament at Cape Mendocino translated through two short meanders before becoming entrained in a mesoscale eddy at the offshore end of its trajectory (39°N, 131°W).

Mesoscale variability (60 – 200 km scales) was most clearly seen by a float that was launched offshore at 37.5°N, 124.5°W. This float initially moved poleward about 100 km before becoming entrained in a large anticyclonic eddy centered about 39°N, 126°W. The radius of the eddy was 71 km and the period 27 days. The eddy translated west-southwest at a mean speed of 0.02 m/s. The float circuited this eddy five times before its mission ended. This eddy appeared highly coherent throughout the water column. AVHRR imagery indicated that the center of the eddy was 1.5°C warmer than the surrounding water. A second float at 1500 dbar was also entrained by this eddy, but the rotation rate at the greater depth was only one quarter of that at 300 dbar.

Ten of the floats underwent anticyclonic motion with a rotational radius in the range of 15-33 km. These appear to be examples of submesoscale coherent vortices (SCVs)(McWilliams, 1985), similar to small eddies (called "meddies") associated with Mediterranean water in the North Atlantic (Armi, et al., 1989; Richardson, et al., 1989). Rotational periods ranged from ten to thirty days and the net west-

ward displacement for floats caught in these small eddies ranged from 0.01 m/s to 0.02 m/s. We speculate that these small eddies entrain equatorial waters and have suggested that they be called California Undercurrent eddies or "cuddies."

Cuddy translation was markedly different from surface flow, as noted above. Once detached from the poleward inshore flow, cuddies moved primarily westward. Trajectories show these eddies being present to at least 127°W, and none of the cuddies showed evidence of decay. To date there are no estimates on how long cuddies exist before collapsing. In the Northeast Pacific, a large variation of the temperature-salinity relationship occurs for intermediate waters at a given location. While some of this variability is associated with intrusive mixing processes, some may also be due to water transport associated with cuddies.

Cuddies appear to form in the Undercurrent and then break away. To date no spatial pattern of preferred formation or detachment locations has been established. Continued observations are trying to quantify cuddy formation. These small eddies represent an important mechanism for offshore transport and mixing along the California coast.

Other Studies

The presence of the sound source array has provided the opportunity for other studies in the Northeastern Pacific Ocean: tracking marine mammals using an acoustic recording tag, tomographic imaging of the California Current, and studies of hydrothermal megaplumes. The acoustic tag was attached to a juvenile northern elephant seal and receipt of RAFOS signals demonstrated the ability to obtain clear records of external signals from swimming marine animals (Burgess, et al., 1997). Tomographic studies of the variations in arrival time of source signals at the Pt. Sur SOSUS array indicated that we need to double the bandwidth of the RAFOS chirp from 1.5 Hz to 3 Hz to be able to distinguish between rays. NOAA researchers using northern California SOSUS arrays have been able to discern seasonal modulations of the California Current using our RAFOS sources.

Megaplumes are formed by the injection of superheated water at locations along the mid-ocean ridge spreading center. Studies of these plumes are occurring on both the Juan de Fuca Ridge and the Gorda Ridge segments of the Pacific mid-ocean ridge. In 1996 RAFOS floats were placed in a hydrothermal plume recently formed over the Gorda Ridge (Lupton, et al., 1998). One float, at a depth of 2200 m, experienced cycloidal motion with a mean radius of 3 km and rotational period of 8.5 days, clearly revealing the anticyclonic motion of the hydrothermal plume. During the 55-day deployment, the float moved northward with a mean speed of 0.03 m/s. These floats confirmed hypotheses (D'Asaro, et al., 1994) that hydrothermal megaplumes are another form of SCVs. The formation of hydrothermal plumes provides a mechanism whereby the injected water can remain as a distinct water parcel for long periods of one to two years. Tagging of these plumes with RAFOS floats allows process studies examining the chemical and biological evolution of the plume.

Summary/Conclusions

The deep ocean is nearly opaque to electromagnetic radiation, although it can be easily ensonified. Acoustically tracked floats provide a method of determining flow paths and mixing patterns. Lagrangian methods provide information on the path taken by a water parcel as well as measurements of dispersal and provide a basis for application to common nautical problems: the drift of a mine or a person who has fallen overboard, or the dilution and mixing of toxic liquids. SCVs and eddies perturb the temperature field and refract sound. Hence, they impact antisubmarine warfare.

The pattern of interior flow that we have observed is deeper and wider than that produced by global numerical eddy resolving ocean models. Regional numerical ocean models produce a more realistic undercurrent: the resulting baroclinic and barotropic instabilities fill the region to the west of the Undercurrent with about equal numbers of cyclonic and anticyclonic mesoscale eddies, but not cuddies. [It is interesting that the floats experienced little cyclonic flow, and it has been speculated that this is due to the divergent nature of cyclonic flow at depth.] The float results suggest the application of a simple advective-diffusive model to Undercurrent flow, $V\, dS/dy = K_x\, d^2S/dx^2$, where V represents poleward flow, S is salinity, x and y are across shore and alongshore coordinates respectively, and K_x parameterizes mixing processes. Evaluating K_x using this equation yields $K_x = 1.3 \times 10^4$ m^2/s; K_x can also be estimated from the variability of float motion which yields 1.9×10^3 m^2/s (Garfield, et al., 1998). The difference may be due to floats becoming trapped within eddies.

The RAFOS system has demonstrated capability as a tool for basic and applied research, opening up many new avenues for research on ocean variability. An incomplete list of some of these opportunities includes studies of the generation and fate of eddies, using sound sources for regional tomography studies, and using isopycnal floats to better understand thermodynamic processes associated with coastal upwelling. By extending the array of sound sources into the Gulf of Alaska, RAFOS floats could also be used to investigate exchanges between North Pacific subtropical and subpolar gyres.

Acknowledgments

This work has been supported by the Office of Naval Research, the Naval Postgraduate School, the Naval Engineering Facilities Command, the National Science Foundation and the National Oceanic and Atmospheric Administration.

Biographies

Professor Curtis Collins received his B.S. degree from the U.S. Merchant Marine Academy and his Ph.D. degree from Oregon State University. His current research is focused on Eastern Boundary Current processes and their effect on maritime and naval operations.

Dr. Newell Garfield received his BA from Williams College, his MS from the University of Delaware and his Ph.D. from the University of Rhode Island. He has been a Research Assistant Professor of oceanography at the Naval Postgraduate School since 1991. His current research interests include observations of ocean circulation using subsurface Lagrangian drifters and satellite data.

Professor Robert Paquette, educated as a physical chemist, entered the field of physical oceanography at the University of Washington in 1947. A descriptive physical oceanographer , he has experience in the Arctic, oceanographic instrumentation and ocean engineering. Now retired, he has recently been working on problems involving RAFOS floats.

Thomas Rago has been an oceanographer at the Naval Postgraduate School since 1987. He obtained his B.A. (Physics) from Amherst College (Massachusetts) in 1979, and his M.S. (Oceanography) from the Graduate School of Oceanography at the University of Rhode Island in 1986.

Dr. Everett Carter received his Ph.D. from Harvard University. After working at the University of Rhode Island and the Naval Postgraduate School, he started his own software company. In addition to oceanography interests, he is an expert in the FORTH language and robotics, and is responsible for code that runs the RAFOS float.

REFERENCES

Armi, L., D. Herbert, N. Oakey, J. Price, P. L. Richardson, T. Rossby and B. Ruddick, 1989, Two years in the life of a Mediterranean salt lens, J. Phys. Oceanogr. 19, 354-370.

Burgess, W. C., P. L. Tyack, B. J. Le Boeuf, and D. P. Costa, 1997, A programmable acoustic recording tag and first results from free-roaming northern elephant seals, submitted to Deep-sea Res.

Brink, K., R. Beardsley, P. Niiler, M. Abbott, A. Huyer, S. Ramp, T. Stanton, and D. Stuart, 1991, Statistical properties of near-surface flow in the California coastal transition zone, J. Geophys. Res. 96, 14693-14709.

Collins, C., N. Garfield, R. Paquette, and E. Carter, 1996, Lagrangian measurement of subsurface poleward flow between 38N and 43N along the West Coast of the United States during Summer, 1993, Geophys. Res. Lett 23, 2461-2464.

D'Asaro, E., S. Walker, and E. T. Baker, 1994, Structure of two hydrothermal megaplumes, J. Geophys. Res. 99, 20361-20373.

Garfield, N., C.A. Collins, R.G. Paquette, and E. Carter, 1998, Lagrangian exploration of the California Undercurrent, 1992-1995, J. Phys. Oceanogr., in press.

Lupton, J., E. Baker, N. Garfield, G. Massoth, R. Feely, J. Cowen, R. Greene and T. Rago, 1998, Tracking the evolution of a hydrothermal event plume using RAFOS neutrally buoyant drifter, under revision for Science.

Lynn, R. and J. Simpson, 1987, The California Current System: The seasonal variability of its physical characteristics, J. Geophys. Res. 92, 12947-12966.

McWilliams, J., 1985, Submesoscale, coherent vortices in the ocean, Rev. Geophys. 23, 165-182.

Richardson, P. L., D. Walsh, L. Armi, M. Schroeder and J. Price, 1989, Tracking three meddies with SOFAR floats, J. Phys. Oceanogr. 19, 371-383.

Rossby, T, D. Dorson and J. Fontaine, 1986, The RAFOS System, J. Atmos. Ocean. Tech. 3, 672-679.

The Real-Time Environmental Information Network and Analysis System (REINAS)

Wendell A. Nuss, Naval Postgraduate School, Monterey, CA
Darrell D.E. Long, Patrick E. Mantey, Alex Pang, and Eric C. Rosen, University of California, Santa Cruz, Santa Cruz, CA
Jeff Paduan, Naval Postgraduate School, Monterey, CA

1. Introduction

Meteorological and oceanographic instrumentation capable of collecting observations of increasing spatial and temporal resolutions as well as the advent of higher resolution numerical models pose significant new challenges to operational and research meteorologists and oceanographers. One significant problem is simply to manage the high frequency and high volume data sets that are becoming routinely available for meteorological forecasting and research. Another significant challenge is to fuse or assimilate a variety of mesoscale observations and a numerical model into an accurate depiction of the atmosphere or ocean for forecasting to support tactical decision making. In addition, methods to combine these different data sets together into a common display for proper diagnostic interpretation by either the operational forecaster or the research meteorologist remains a significant challenge. The Real-time Environmental Information Network and Analysis System (REINAS) addresses these and other issues through a complete end-to-end system approach.

The REINAS project is an Office of Naval Research (ONR) sponsored University Research Initiative (URI) aimed at developing computer technology to manage real-time, high-frequency, high-volume observational data sets. The project began in late 1992 and is a collaborative effort between the University of California, Santa Cruz (UCSC), the Naval Postgraduate School (NPS), and the Monterey Bay Aquarium Research Institute (MBARI). The project has focused primarily on the computer technology but has provided a catalyst to develop a multi-disciplinary mesoscale

observing network for the California coastal region that supports the development and testing of tactical scale environmental analysis techniques.

2. The System Description

The REINAS computer technology rests on the use of relational database technology and the use of Internet protocols to provide robust data passing between the distributed nodes. Fig. 1 provides a schematic view of the core REINAS system architecture, which shows that REINAS is logically composed of three subsystems. The three subsystems are the instrumentation or data collection subsystem, the database subsystem, and the user access, analysis and display subsystem (analysis subsystem). Each of these logical subsystems is distributed over a number of actual computer systems through network connectivity via the Internet. Specific computations are distributed to the most appropriate location within REINAS and its attendant subsystems. The relational database, shown in the center of Fig. 1, is a commercially available database (ORACLE) to which the REINAS system is attached. More details about the REINAS technology can be found in Rosen et al (1997) and on the web site, http://csl.cse.ucsc.edu/reinas.

Figure 1
REINAS Logical Architecture.

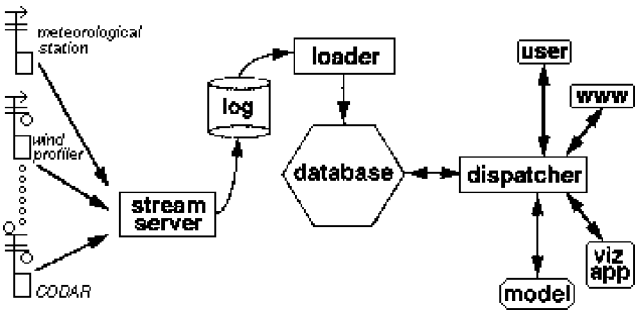

a. The Collection Subsystem

The collection or instrumentation subsystem consists of the observation sources to be loaded into the REINAS database. These sources include but are not limited to routine meteorological observations received as WMO bulletins, surface mesonet stations, 915 and 404 MHz wind profilers, CODAR, satellite images, numerical model fields, and NEXRAD data. Individual instruments, which may be actual sensors or observation files fed from elsewhere, are connected to a stream server on the database node through

Figure 2
Monterey Bay observing network consisting of surface meteorological stations, wind profilers, a NEXRAD, and ocean radars (CODAR). Individual observation sites are maintained by various different agencies in the area.

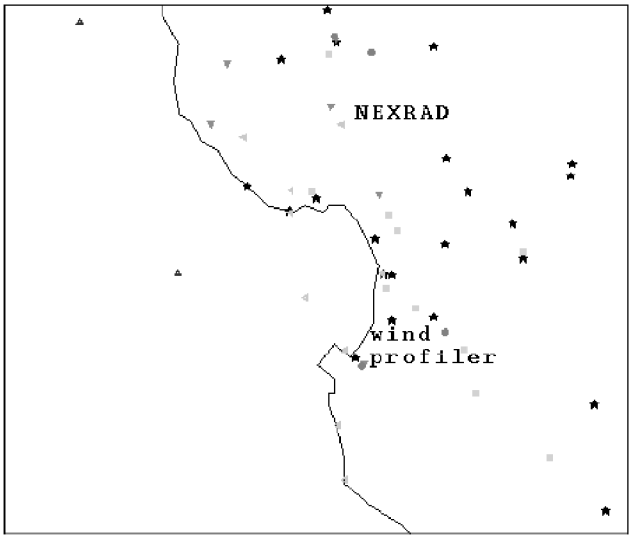

standard Internet connections as well as radio modems and ISDN phone connections. The basic model that describes the collection subsystem is that each instrument consists of a microcomputer that writes data to a log, converts it to a common format, and transmits the data to the database subsystem. Each instrument is consequently a stand alone system capable of storing its inherent data stream for some period of time determined by microcomputer specifications. This ensures no data loss during communications link failures as the stored data in the instrument log is simply loaded into the database after the connection is reestablished. Another key component of this technology is that the Internet Protocol is a robust networking standard that ensures no loss in the transmission of data from instrument to database. These aspects provide a data collection system that can not lose data as long as the instrument is running, even when the communications link may temporarily fail.

A major out-growth of REINAS has been the development of a coastal mesoscale observing network (mesonet). Through the REINAS project, many existing oceanographic and meteorological observing sites for the Monterey Bay area have been collected together into a mesonet as seen in Fig. 2. These have included standard National Weather Service (NWS) observation sites plus sites run by NPS and other research organiztions in the area. The REINAS project has also deployed some instrumentation to provide a more complete observing system. Not all data goes into REINAS in real-time due to a variety of issues but these are being worked on.

b. The Database Subsystem

The database subsystem consists of a variety of processes used to manage, load, and retrieve data in a relational database. Key components of the database subsystem are the loader module and dispatcher. The loader is a software component that handles the real-time insertion of data into the database. A key aspect of this technology is its ability to handle rapid loading of large volumes of data efficiently into the database. Standard database technology is incapable of writing high volumes of data in real-time as it has been designed primarily for long-term storage not real-time loading. Upstream from the loader is the stream server that acts to collect the various observational data streams to be feed into the database. The other key element is the dispatcher, which provides a relatively user friendly query interface to the REINAS database. The dispatcher uses some canned query tools to support most typical meteorological applications. SQL, or Structured Query Language, can be used to interact with the database as well but most users are not likely to develop SQL queries and can use the set of standard dispatcher commands. The components of the database subsystem can be distributed across platforms to form a federated database.

Critical to the database subsystem is an information model used to generate the metadata used in the database subsystem to support queries. Metadata consist of the information about the data content, context, structure as well as instrument engineering information. The database subsystem makes use of this information to support not only queries about the observations themselves but also the quality of the observation, the engineering or calibration information and numerous other instrument related items that may be of interest to scientists or instrument engineers responsible for design or maintenance.

c. The Analysis Subsystem

The analysis subsystem has two major components. The first component is a data assimilation and modeling component and the second component is a visualization package developed for the simultaneous exploration and display of meteorological and oceanographic data. A major purpose behind the development of REINAS is to provide the observational and historical data management task associated with local tactical-scale modeling efforts. The REINAS system provides the observational input to a mesoscale data assimilation system as well as providing for the storage of model output. Key components of this system are being used in a real-time local modeling effort at NPS using the NCAR/Penn State MM5 model. Observations are collected and managed using the REINAS system which then feeds them into the mesoscale data assimilation system (described in more detail later) being developed to use with the MM5 or Navy's Coupled Ocean and Atmosphere Mesoscale Prediction System (COAMPS) models. A key aspect of using REINAS to manage the mesoscale observations is that the data management for high volume data streams such as satellite images and NEXRAD data are handled efficiently and can be easily recalled for insertion into the model as well as post analysis work.

Although REINAS will support the application of many visualization packages through an application program interface (API), the primary tool used for data displays was developed as part of REINAS. As part of REINAS, the Santa Cruz Laboratory of Visualization and Graphics (SLVG) at UCSC has developed a set of tools to visualize environmental data as collected in REINAS. This visualization package, referred to as SLVG, is capable of mixing observations, model products, and satellite imagery into a single visualization in three dimensions. The interface is a straight forward X-windows system that allows the user to build his visualization products using a set of defined tools. These tools are used to build isosurfaces, contours, three dimensional volumes, satellite images, station observation displays, vertical profiles, and other products using a variety of observational and model data stored in the REINAS database. SLVG is tied directly to the database and executes its own queries based on the visualization request, which provides a simple mode for the user to interact with the database. An example of a product developed using SLVG is shown in Fig. 3, where surface observations, coastal wind profilers and research aircraft observations are displayed along with an isosurface of the California coastal topography. The view is interactive and can be rotated to better observe the structure of the atmosphere represented in the visualization product.

Another aspect of the analysis subsystem has been the development of a simple World Wide Web (WWW) based data browser and query system. The WWW provides an ex-

Figure 3
Three dimensional visualization of the California topography (isosurface) and various observation platforms supported in REINAS. Wind profilers are the vertical stacks of vectors, an aircraft track with wind vectors along a single portion of the track.

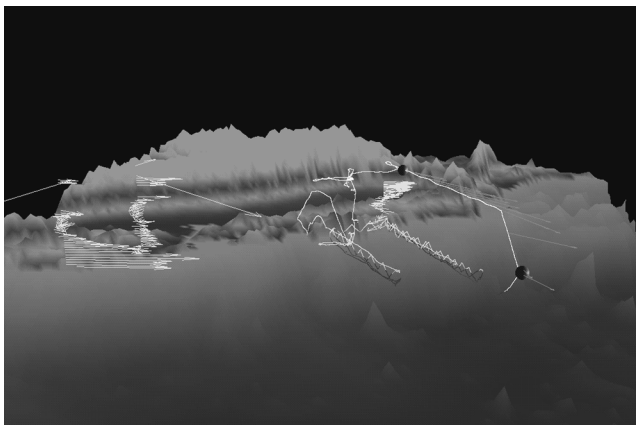

cellent mechanism by which both casual non-scientific users and professional meteorologists or scientists can obtain simplified access to query the data base and display the results using simple graphics. This user interface has become very popular to a large body of more casual users of REINAS mesonet data. Current winds, precipitation, and most of the scientific variables stored in REINAS can be viewed using the WWW query system.

3. Environmental Applications

A key aspect of the REINAS project from a meteorological perspective has been to examine how best to use mesonet data in a region of complex coastal topography. Science studies to better understand the physical mechanisms forcing the atmosphere over the Monterey Bay as well as to examine how to assimilate these observations into a mesoscale model have been a major focus. The impact of mesonet data on the model forecasts and the proper use of these observations for mesoscale forecasting are two areas where REINAS mesonet data are actively being used.

To demonstrate the need for mesonet observations in order to more completely describe the atmosphere around the Monterey Bay region, a forecast from the Coupled Ocean and Atmosphere Mesoscale Prediction System (COAMPS) of the Naval Research Lab is shown in Fig. 4. This forecast is from a relatively typical summer day along the California coast during which a sea breeze circulation develops through the day. The forecast illustrates several key questions about the use and generation of tactical scale forecasts.

First, while the forecast may be physically plausible, the accuracy is unknown and difficult to assess due to a lack of small scale observational data. The accuracy may be sensitive to the depiction of larger-scale features in the model initial conditions as well as details in the observed small scale structures. Second, the ability of a model to utilize mesoscale observations, if they are available, is not known and is highly dependent upon the nature of the data assimilation used by the model. One of the goals of the REINAS project was to develop tools that may address these small scale forecast issues.

To illustrate some of these small scale forecast problems as well as some of the tools developed as part of REINAS, the 9 km resolution COAMPS 9 hour forecast on this sea breeze day in June 1996 (Fig. 4) is examined in more detail. The limitations in the model, run at this resolution, to fully describe the Monterey Bay sea breeze and its variations around the bay are evident in the figure. The high resolution model shows a pronounced coastal thermal gradient but misses some details in the wind field that are seen in even the few observations plotted in Fig. 4. While these differences appear to be small (vector errors less than 5 m/s),

Figure 4
COAMPS 9 hour forecast for the Monterey Bay region during a sea breeze situation. Surface temperature (color fill contours) and surface winds (barbs) are shown with some mesonet observations.

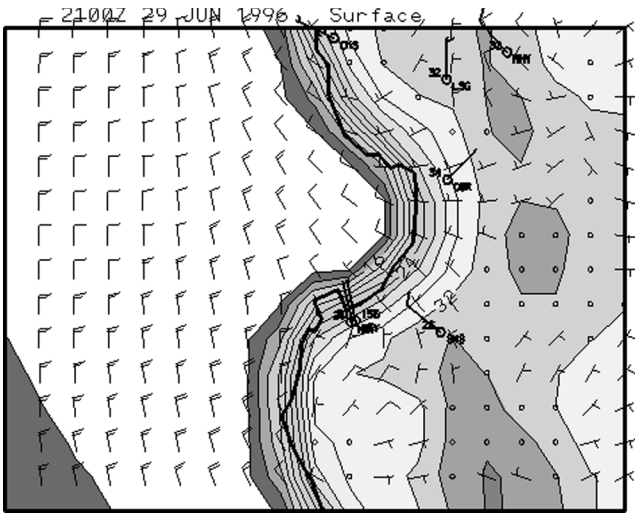

their impact on the surface convergence and height of a capping marine layer inversion are important. Results from studies (Nuss, 1998) involving many more days suggest that the sea-breeze driven surface wind convergence and divergence can be associated with marine boundary layer depth changes and stratus clearing. As will be shown in a subsequent figure, the COAMPS thermal structure rather poorly represents real differences in the thermal structure that occur in the north and south parts of the Monterey Bay. While these differences are not large, they do explain differing evolutions in the observed and model forecast surface winds and associated boundary layer structure.

To assist in the real-time assessment of a mesoscale model forecast, such as that depicted in Fig. 4, the SLVG visualization software contains several tools directly aimed at monitoring the growing uncertainty or error in a model forecast. Djurcilov and Pang (1997) describe these tools which allow the display of model error relative to real-time observations as two dimensional pseudo-color surfaces, station point value depictions, iso-contours, volume probes and other techniques. These visualizations depict the areas in the model where growing model uncertainty will contribute to poor forecasts. While these visualizations of model error are helpful in assessing the model, perhaps more important to a forecaster is the ability to monitor the evolution of the atmosphere from the disparate collection of observations in REINAS, which can be accomplished by combining the observations in a local-scale analysis.

To demonstrate the application of REINAS mesonet data to real-time mesoscale analysis and mesoscale modeling in complex terrain, the sea breeze example shown in

Fig. 4 was analyzed using a 3-dimensional multiquadric interpolation-based (3D MQ) analysis system developed at NPS as part of REINAS. The three dimensional multiquadric interpolation blends a model supplied first guess field with available observations in three dimensions. The application of multiquadric interpolation to meteorology is described in Nuss and Titley (1994), where the approach is shown to belong to a mathematical class of interpolation techniques referred to as radial basis function interpolation. Optimum interpolation is another well-known member of this class of mathematical techniques. The 3D MQ used for this analysis was run in a univariate sense and interpolates the three dimensionally scattered data to a specified output grid. Surface data in complex terrain are treated three dimensionally by accounting for their vertical location in height coordinates.

The application of 3D MQ to the mesoscale analysis using all the available REINAS mesonet data for the June 1996 sea breeze case discussed above is shown in Fig. 5. In this analysis, the National Centers for Environmental Prediction (NCEP) ETA model was used as a first guess and then blended with the mesoscale observations using 3-D multiquadric interpolation. A major difference in the analysis, compared to the COAMPS forecast, is that the coastal thermal gradient is indeed along the coast and there are differences in its intensity in the north and south parts of Monterey Bay. In fact, detailed analyses through the day depict the development of a sea breeze front in the south part of the Monterey Bay, which advects inland and weakens through the day. The 2100 UTC analysis shown in Fig. 5 contrasts sharply with the over simplified surface forecast from the 9 km resolution COAMPS model shown in Fig. 4. Realistic features such as the warm temperatures over the Santa Cruz mountains just north of the bay or in the upper parts of the Salinas valley in the lower right corner as well as the weakening sea breeze front near Salinas (SNS) are very nicely represented in the mesoscale analysis. The analyzed wind field also shows stronger west winds in the north part of the bay and a stronger sea breeze near Salinas than the COAMPS forecast. These wind differences are in accord with the thermal structure differences, which highlights the value of obtaining the mesoscale analysis compared to even a short term model forecast.

Figure 5
Mesoscale analysis for 29 June 1996 using 3D MQ with all mesonet observations.

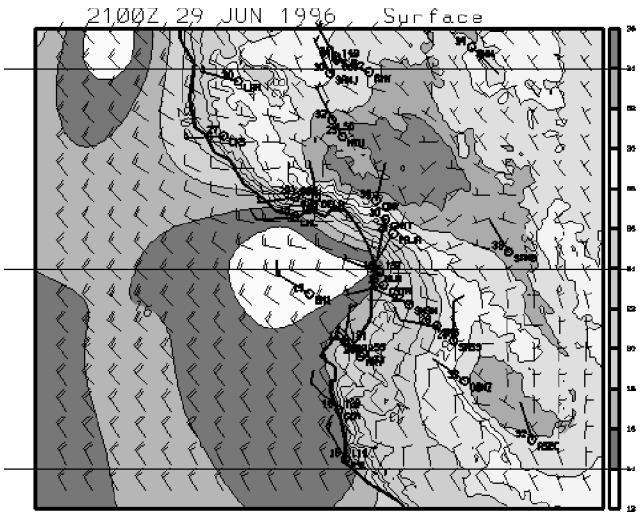

Figure 6
Surface wind analysis from REINAS observations for June 21, 1996 overlaid on GOES-9 satellite image.

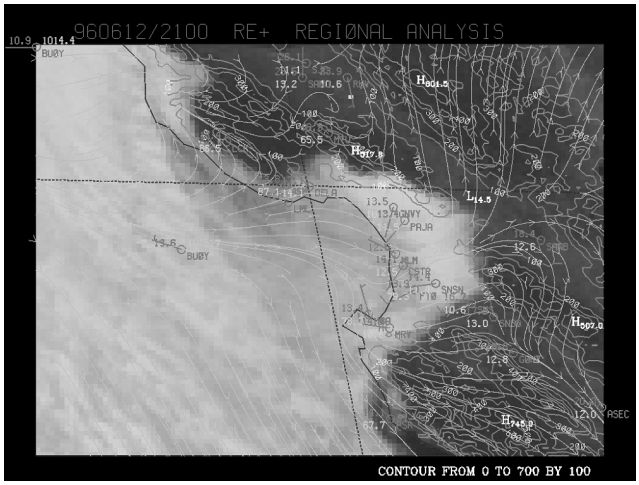

The 3DMQ mesoscale analysis software is coupled to the REINAS database, which allows real-time observational analysis. This illustrates one of the advantages of the end-to-end nature of the REINAS system. The data collection subsystem is gathering observations immediately from the distributed instruments that use the REINAS approach (some low rate data such as WMO bulletins are delivered via less timely approaches). Consequently, the data become available for rapid assimilation or analysis using the 3DMQ software coupled directly to the database subsystem. An example of frequent real-time mesoscale analysis is a surface wind analysis that is run every hour using the REINAS data and the 3DMQ analysis system. An example of the results are shown in Fig. 6, where the winds are displayed on a satellite image to help illustrate the relationship between the wind and low-level stratus in the Monterey Bay. Although less important for the real-time forecaster, another distinct advantage of REINAS is the ease with which historical observations can be retrieved and used in the same analysis system. Thus re-analysis for research or to examine analog events is easily done.

Another key aspect of REINAS is that the system includes both atmospheric and oceanic observations. This multi-disciplinary data set brings together the environmen-

tal information needed to simultaneously examine the coastal atmosphere and ocean. The primary ocean information presently being collected in REINAS is observations from multiple coastal high frequency radars (CODAR), which measure the near surface ocean currents. Paduan and Rosenfeld (1996) describe the utility of CODAR measurements to observe two-dimensional current fields in the Monterey Bay region. Real-time monitoring of these currents is also possible using REINAS, and these ocean observations can be viewed in a common display with meteorological observations and model output using the SLVG visualization tools. Although at present the ocean observations are limited, other data sources, such as satellite imagery or moored, ship-based, or coastal observations, can be easily incorporated in real time, provided the requisite telemetery links are in place. In this way, REINAS demonstrates the possibilities for combining various multi-disciplinary data sets together to improve the real-time description of a tactical-scale environment.

4. Summary

REINAS is a distributed and extensible end-to-end system designed for complete management of meteorological and oceanographic data. The system utilizes networking running Internet protocols to connect the distributed parts in a robust complete system, which includes instrument systems, computer systems running database software, and systems that run a variety of application programs. Although other environmental database systems exist, REINAS provides the ability to effectively utilize the database technology in real time with voluminous and high frequency environmental data.

The REINAS system has been developed for the Monterey Bay region in order to develop and test mesoscale analysis and forecasting approaches including both the atmosphere and ocean. Mesoscale analysis software has been developed and used for local small scale analysis as well as to initialize mesoscale forecast models. Visualization tools allow the user to produce combined displays of model, observations, and imagery into a common depiction of the coastal atmosphere and ocean. Tools to monitor the growth of mesoscale model errors, display three dimensional observations from multiple sources, as well as more routine horizontal depictions of model or gridded analysis fields have been developed.

Further testing of the current system as well as the development of appropriate tools for specific applications will continue in the future. Key development areas include improvements to the mesoscale analysis system to utilize dynamic balances in the analysis and visualization tools to highlight critical mesoscale circulation features such as the height of the inversion. Expansion of the data stream feeding into REINAS is also being pursued through several related projects.

5. Biographies

Dr. Wendell A. Nuss is an Associate Professor in the Department of Meteorology, Naval Postgraduate School. Since joining the faculty, he has participated in two major field projects in extratropical cyclogenesis and lead a field program in coastal meteorology. During 1987, he was awarded a Postdoctoral Fellowship by the Japan Society for the Promotion of Science to study at the Ocean Research Institute, Tokyo University. Since returning to the Department he has been actively pursuing research on extratropical cyclogenesis, objective analysis techniques and coastal meteorology.

Dr. Darrell Long is Associate Professor of Computer Science at the University of California, Santa Cruz. The department is now part of the new Jack Baskin School of Engineering. He received his B.S. degree in Computer Science from San Diego State University in 1984, and his M.S. and Ph.D. degrees in Computer Science and Engineering from the University of California, San Diego in 1986 and 1988 respectively. His research interests include distributed systems, particularly high speed storage systems, fault tolerance, performance evaluation and mobile computing. He directs the Concurrent Systems Laboratory in the Baskin Center for Computer Engineering and Computer Science.

Dr. Pat Mantey is the Dean of the new Jack Baskin School of Engineering at the University of California, Santa Cruz after having served as a Professor and Department Chair for Computer Engineering. He obtained his Ph.D. from Stanford University in 1965 and an M.S. from University of Wisconsin. His research interests are in image systems, multimedia electronic libraries, image processing, graphics, workstation architecture, systems, digital signal processing, real-time control.

Dr. Alex Pang is an Associate Professor in the Computer Sciences Department at University of California, Santa Cruz. He obtained his M.S. and Ph.D. in Computer Science from UCLA in 1984 and 1990. His current research interests are in collaboration software, uncertainty visualization, scientific visualization, and virtual reality interfaces.

Dr. Eric C. Rosen contributed to the design and implementation of REINAS, as well as the day-to-day management and ongoing development of the operational system. His broad interests include wireless telecommunications, large network systems, digital video and spread-spectrum applications. He is a member of the IEEE.

Dr. Jeffrey D. Paduan received his Ph.D. from Oregon State University in 1987. Since joining the NPS faculty in 1991, he has initiated a program using HF radars to remotely measure ocean surface currents. His focus is on improving HF radar performance, while describing the dominant current processes in Monterey Bay.

6. REFERENCES

Djurcilov, S. and A. Pang, 1997: Visualization tools for data assimilation, *SPIE'97 Conference on Visual Data Exploration and Analysis*.

Nuss, W.A., 1998: Diurnal variability of the coastal winds in the Monterey Bay. *in preparation*.

Nuss, W.A. and D.W. Titley, 1994: Use on multiquadric interpolation for meteorological objective analysis. *Mon. Wea. Rev.*, **122**, 1611-1631.

Paduan, J.D., and L.K. Rosenfeld, 1996: Remotely sensed surface currents in Monterey Bay from shore-based HF radar (CODAR). *J. Geophys. Res.*, **101**, 20669-20686.

Rosen, E.C., T.R. Haining, D.D.E. long, P.E. Mantey, C.M. Wittenbrink, 1997: REINAS: A real-time system for managing environmental data. *J. Software Engr. and Knowl. Engr.*

Toward Accurate Coastal Ocean Prediction

Peter C. Chu, Department of Oceanography, Naval Postgraduate School, Monterey, CA

1. Introduction

Several major problems, namely, uncertain surface forcing, unknown open boundary conditions (OBC), and pressure gradient error using the σ-coordinate, restrict the accuracy of littoral zone ocean prediction.

The littoral zone ocean prediction is usually proceeded by integrating a set of dynamic/thermodynamic equations from initial states under the surface wind forcing

$$\rho_0 K_H \left(\frac{\partial u}{\partial z}, \frac{\partial v}{\partial z} \right)_{z=0} = \left(\tau_{0x}, \tau_{0y} \right) \qquad (1)$$

the surface thermal forcing

$$K_H \frac{\partial T}{\partial z} |_{z=0} = \alpha_1 \left(\frac{Q_H}{\rho c_p} \right) + \alpha_2 \kappa \left(T_{0BS} - T_0 \right) \qquad (2)$$

$$K_S \frac{\partial S}{\partial z} |_{z=0} = \alpha_1 Q_S + \alpha_2 \kappa \left(S_{0BS} - S_0 \right) \qquad (3)$$

and the lateral boundary conditions. Here (u, v) and (τ_{0x}, τ_{0y}) are the two components of the water velocity and wind stress vectors, T_{OBS} and S_{OBS} are the observed temperature and salinity, T_0 and S_0 are the surface temperature and salinity, c_p is the specific heat, and Q_H and Q_S are surface net heat and salinity fluxes, respectively. The coupling coefficient κ is the reciprocal of the restoring time period for a unit volume of water. The parameters (α_1, α_2) are (0,1)-type switches: $\alpha_1=1$, $\alpha_2=0$, would specify the flux forcing; $\alpha_1=0$, $\alpha_2=1$, would specify the restoring-type forcing. The restoring-type forcing, called Haney-type surface boundary condition (Haney, 1971), was obtained under the assumption that the ocean is in contact with an atmospheric equilibrium state (i.e., an atmosphere with a near-infinite heat capacity). The validity of the restoring-type condition need to be verified.

At open lateral boundaries where the numerical grid ends, the fluid motion should be unrestricted. Ideal open boundaries are transparent to motions. Two approaches, local-type and inverse-type are available for determining OBC. The local-type approach is to select an OBC from a set of *ad hoc* OBCs, which will introduce inaccuracies into a nu-

merical solution (Chapman 1985). The inverse-type approach is to determine the OBC from a "best'' fit between model solutions and interior observations. The most popular and successful scheme for this approach is an adjoint method (Robinson, 1993; Seiler 1993; Gunson and Malanotte-Rizzoli 1996). The disadvantages that may restrict use of adjoint method are: ocean-model dependency of the adjoint equation, and difficulty in deriving the adjoint equation when the model contains rapidly changing (discontinuous) processes, such as ocean mixed layer dynamics. To overcome such deficiencies, Chu et al. (1997) have developed an inverse method to determine OBCs of ***any ocean model*** from interior observations by seeking a relationship among three vectors: open boundary parameter vector (**B**), observation vector (**O**), and solution vector (**S**).

How to reduce the horizontal pressure gradient error is another key issue of using σ-coordinate ocean models, especially of using coastal models. The error is caused by the splitting of the horizontal pressure gradient term into two parts and the subsequent incomplete cancellation of the truncation errors of those parts. Due to the fact that the higher the order of the difference scheme, the less the truncation error and the more complicated the computation, Chu and Fan (1997a,b; 1998) have used and developed several high-order schemes for ocean models without drastic increase of CPU time.

2. Uncertainty of Surface Forcing

To verify the validity of Haney-type surface thermal boundary conditions, Chu and his colleagues computed cross correlation coefficient (CCC) between Q_H and ΔT [= (T_{OBS} - T_0)] using the NCEP global re-analyzed data (six hour resolution) during 1 October 1994 - 31 December 1995 (Chu et al., 1998a) and using a coupled atmosphere-ocean model developed at the Institute for Space Studies at NASA/Goddard Space Flight Center (Chu, et al., 1998b). The ensemble mean CCC fields show (a) no correlation between Q_H and ΔT in the equatorial and coastal regions, and (b) evident correlation ($CCC \geq 0.7$) between Q_H and ΔT in the middle and high latitude open ocean regions. The variance analysis suggests a value of 70 W m^{-2} K^{-1} (65 W m^{-2} K^{-1}) for the coefficient κ in the northern (southern) middle and high latitude zone.

To investigate the uncertainty in the surface wind forcing and its effect on the coastal prediction, the Princeton Ocean Model (POM) developed by Blumberg and Mellor (1987) was used with 20 km horizontal resolution and 23 sigma levels conforming to a realistic bottom topography during the life time of tropical cyclone Ernie 1996 (Figure 1) over the South China Sea (SCS). Numerical integration was divided into pre-experimental and experimental stages. During the pre-experimental stage, the POM was integrated for 43 months from zero velocity and April temperature and salinity climatological fields with climatological monthly mean wind stresses, restoring type surface salt and heat, and observational oceanic inflow/outflow at the open boundaries. The fields at the end of the integration period were taken as the initial fields (1 November) for the sensitivity study. During the experimental stage, the POM was integrated for another month under the NCEP re-analyzed surface fluxes along with two surface wind data sets: namely, the daily averaged interpolated NASA Scatterometer (NSCAT) winds and the

Figure 1
The track of the tropical cyclone Ernie 4-18 November, 1996 (from Chu et al., 1998).

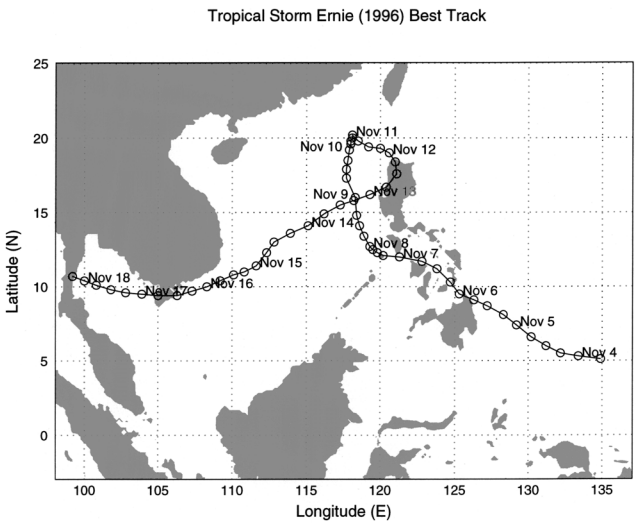

Figure 2
Temporally varying root-mean-square difference between daily mean NSCAT and NCEP winds over the whole South China Sea (from Chu et al., 1998).

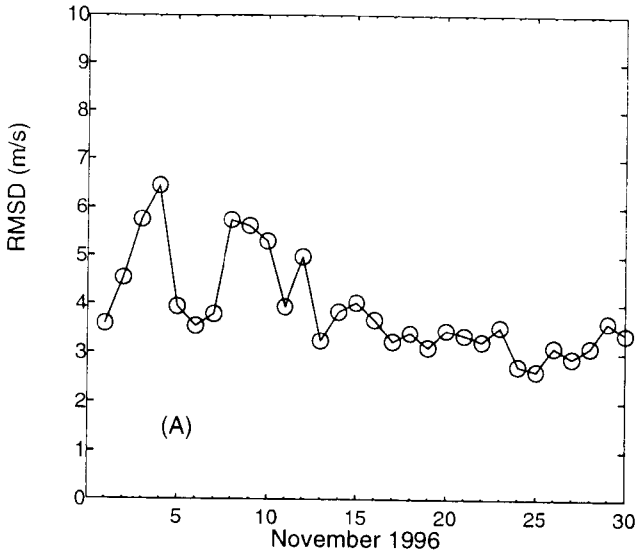

NCEP winds. All the surface forcing data used were from 1 to 30 November 1996. The study (Chu, et al, 1998c) shows that the root-mean-square (RMS) difference of each component (zonal or latitudinal) between the two wind data over the whole SCS during November 1996 fluctuated between 2.7 m/s to 6.7 m/s (Figure 2). The uncertainty of the whole SCS response to the two wind data sets were 4.3 cm for surface elevation (Figure 3a), 0.16 m/s for surface current velocity (Figure 3b), and 0.5°C for near-surface temperature (Figure 3c), respectively.

3. Optimization Method for Determining OBCs

Improvement of the prediction partially depends on the determination of lateral OBCs. If r denotes the position of any point along the open boundary Γ, the boundary values of any variable η are described by a function of r, $\eta^{(b)} = \eta^{(b)}(r)$. Let $f_1(r), f_2(r), \ldots, f_n(r)$ be a series of known basis functions. We expand the function $\eta^{(b)}(r)$ into

$$\eta^{(b)}(r) = \sum_{i=1}^{n} b_i f_i(r) \qquad (4)$$

Figure 3
Temporally varying root-mean-square difference between model results under two kinds of wind forcing over the whole South China Sea (from Chu et al., 1998): (a) surface elevation, (b) current velocity, and (c) temperature.

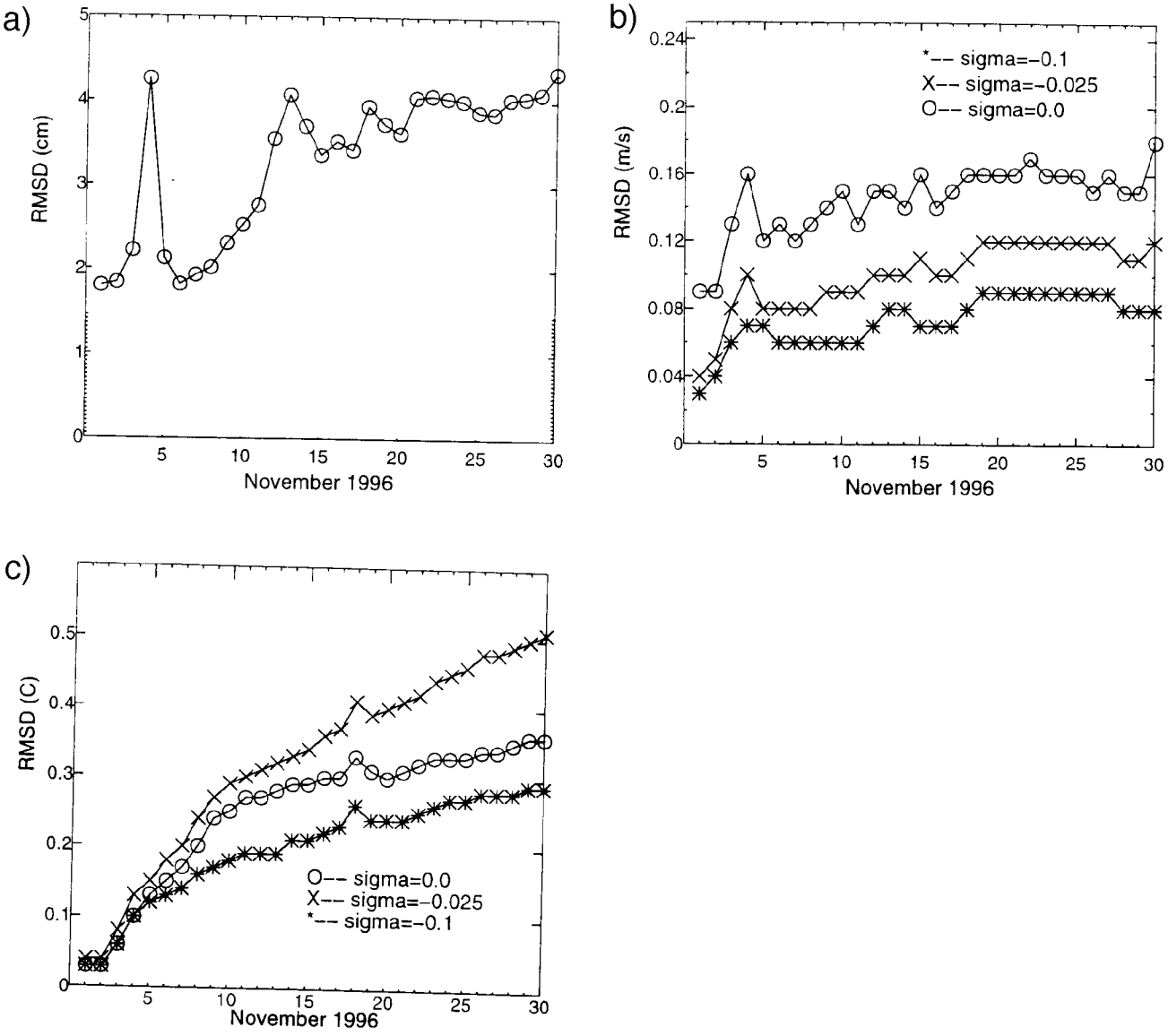

Figure 4
Can open boundary condition be determined from interior values? (from Chu et al., 1997).

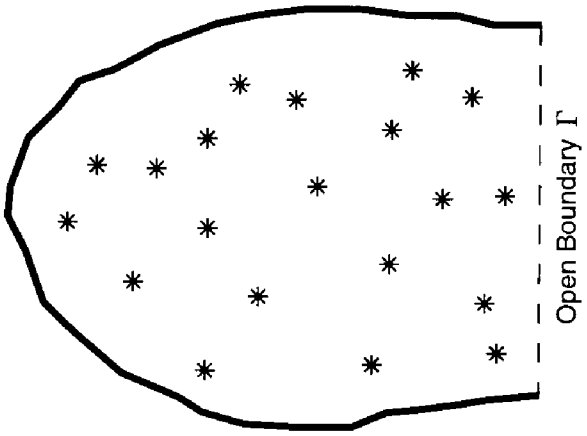

Thus, the determination of the open boundary condition $\eta^{(b)}(r)$ becomes the determination of a n-dimensional boundary vector **B** = (b_1, b_2, ..., bn). Assume that there are *m* observations, forming a m-dimensional vector (observation vector) **O** = (O_1,O_2,..., O_m), located at the interior (Figure 4). If **B** is given, we can solve the dynamic system and obtain the solution **S**. At the same locations where the observations take place, the solutions form a solution vector **S** =(S_1, S_2, ..., S_m). Notice that the dimension of **B** is not necessary the same as the dimension of **O** and **S**.

The optimization method is used to find **B** = (b_1, b_2, ..., bn) by minimize the root-mean-square (RMS) error

$$I = \sqrt{\frac{1}{m}\sum_{j=1}^{m}(S_j - O_j)^2} \qquad (5)$$

This method was verified by a flat bay centered at 35°N and bounded by three rigid boundaries (Chu et al., 1997). This bay expands 1000 km in both the north-south and east-west directions. The northern, southern, and western boundaries are rigid, and the eastern boundary is open. Using the optimization method, the temporally varying OBC, ***B***(t), is determined. After 10 day's of integration, the magnitude of relative error $E^{(O)}$ is on the order of 10^{-4}-10^{-5} (Figure 5). Chu et al. (1997) also pointed out that smoothing on $\delta\boldsymbol{B}$ is very important for this method. This optimization method performs well even when random noises are added to the 'observational' points. This indicates that we can use real-time data to invert for the unknown open boundary values.

Figure 5
Relative error of the inverse method (from Chu et al., 1997).

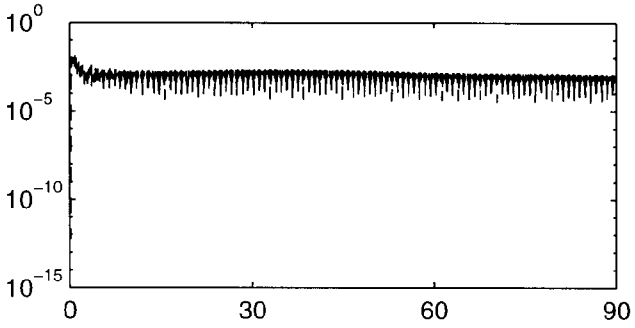

4. High-Order Difference Schemes

4.1 A Hidden Problem

Improvement of the prediction also partially depends on the selection of the discretization schemes. Most coastal models use second-order difference schemes (such as second-order staggered C-grid scheme) to approximate first-order derivative (Blumberg and Mellor, 1987; Hadivogel et al., 1991)

$$\left(\frac{\partial p}{\partial x}\right)_i \cong \frac{p_{i+1/2} - p_{i-1/2}}{\Delta} - \frac{1}{24}\left(\frac{\partial^3 p}{\partial x^3}\right)_i \Delta^2 \qquad (6)$$

where p and Δ represent pressure and grid spacing. Such a difference scheme was proposed by numerical modelers in early 50's as the first generation computers came into place. Since then, the computer upgrades rapidly with several orders of magnitude increase in computational power. However, the difference schemes used by most modelers now are still staying at the 50's level (second-order schemes). Besides, the current scheme uses the local Lagrangian Polynomials whose derivatives are discontinuous. Figure 6 shows the process of computing first-order derivative of function $\phi(x)$ at the grid x_i. $L'(x_i)$ is the tangential of the Lagrangian Polynomial. As i increases, three neighboring Lagrangian Polynomials L_{i-1}, L_i, L_{i+1} have different tangentials at the point x_i. Such a hidden problem might distort the physical process. In some series of papers, Chu and Fan (1997a, b) have shown the advantage of using high-order schemes.

Figure 6
Discontinuity of the first derivatives of the Lagrangian Polynomials at each grid point.

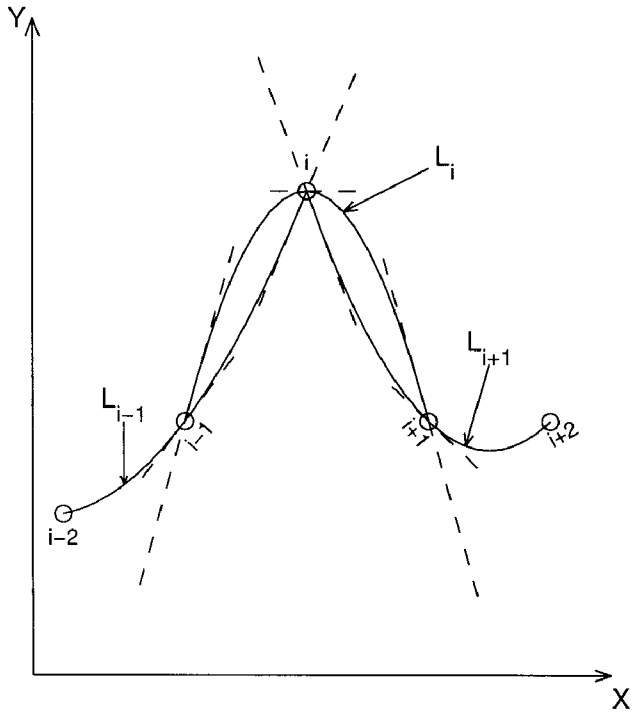

4.2 Combined Compact Scheme

Recently, Chu and Fan (1998) proposed a new three-point combined compact difference (CCD) scheme,

$$\left(\frac{\delta f}{\delta x}\right)_i + \alpha_1\left[\left(\frac{\delta f}{\delta x}\right)_{i+1} + \left(\frac{\delta f}{\delta x}\right)_{i-1}\right] + \beta_1\Delta\left[\left(\frac{\delta^2 f}{\delta x^2}\right)_{i+1} - \left(\frac{\delta^2 f}{\delta x^2}\right)_{i-1}\right] + \ldots = \frac{a_1}{2\Delta}\left(f_{i+1} - f_{i-1}\right)$$

$$\left(\frac{\delta^2 f}{\delta x^2}\right)_i + \alpha_2\left[\left(\frac{\delta^2 f}{\delta x^2}\right)_{i+1} + \left(\frac{\delta^2 f}{\delta x^2}\right)_{i-1}\right] + \beta_2\frac{1}{2\Delta}\left[\left(\frac{\delta f}{\delta x}\right)_{i+1} - \left(\frac{\delta f}{\delta x}\right)_{i-1}\right] + \ldots = \frac{a_2}{\Delta^2}\left(f_{i+1} - 2f_i + f_{i-1}\right) \qquad (7)$$

to compute f_i', f_i'',..., $f_i^{(k)}$ by means of the values and derivatives at the two neighboring points. Moving from the one boundary to the other, CCD forms a global algorithm to compute various derivatives at all grid points, and guarantees continuity of all derivatives at each grid point.

4.3 Seamount Test Case

Model Description

Suppose a seamount located inside a periodic *f*-plane ($f_0 = 10^{-4}$ s^{-1}) channel with two solid, free-slip boundaries along constant y. Unforced flow over seamount in the presence of resting, level isopycnals is an idea test case for the assessment of pressure gradient errors in simulating stratified flow over topography. The flow is assumed to be reentrant (periodic) in the along channel coordinate (i.e., *x*-axis). We use this seamount case of the Semi-spectral Primitive Equation Model (SPEM) version 3.9 to test the new difference scheme. The reader is referred to the original reference (Haidvogel et al., 1991) and the SPEM 3.9 User's Manuel (Hedstrom, 1995) for detail information. The time step and grid size used here are,

$$\Delta t = 675s, \Delta x = \Delta y = 5km.$$

Topography

The domain is a periodic channel, 320 km long and 320 km wide. The channel walls are solid (no normal flow) with free-slip viscous boundary conditions. The channel has a far-field depth h_{max} and in the center it includes an isolated Gaussian-shape seamount with a width *A* and an amplitude h_s (Figure 7),

$$h(x,y) = h_{\max} - h_s \exp\left[-\frac{(x-x_0)^2 + (y-y_0)^2}{A^2}\right] \qquad (8)$$

where (x_0, y_0) are the longitude and latitude of the seamount center. The far-field depth (h_{max}) is fixed as 5,000 m. But the seamount amplitude (h_s) changes from 500 to 4,500 m, and the lateral scale of the seamount (*A*) varies from 10 to 40 km for this study.

Figure 7
Seamount geometry (from Chu and Fan, 1997a,b).

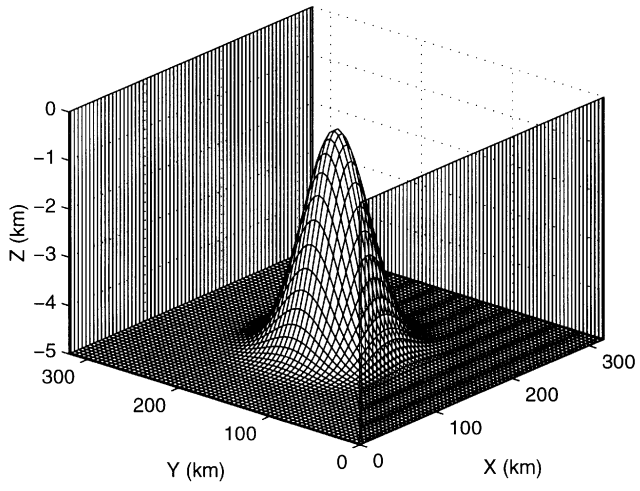

Density Field

The fluid is exponentially stratified and initially at rest. The initial density field has the form,

$$\rho_i = \overline{\rho}(z) + \hat{\rho}\exp\left(\frac{z}{H_\rho}\right) \qquad (9)$$

where z is the vertical coordinate, and H_ρ =1000 m, and

$$\overline{\rho}(z) = 28 - 2.0\exp\left(\frac{z}{H_\rho}\right) \qquad (10)$$

is a reference density field. Here a constant density, 1000 kg m^{-3}, has been subtracted for the error reduction. Following Beckmann and Haidvogel (1993) and McCalpin (1994), we subtract the mean density field $\overline{\rho}(z)$ before integrating the density field to obtain pressure from the hydrostatic equation.

The density anomaly, $\hat{\rho}$, indicates that the initial condition of the model was slightly less stably stratified than the reference field for each computation. In this study, the density anomaly varies from 0.1-1 kg m^{-3}.

4.4 Temporal Variations of Peak Error Velocity

Owing to a very large number of calculations performed, we discuss the results exclusively in terms of the maximum absolute value the spurious velocity (called peak error velocity) generated by the pressure gradient errors. Figure 8 shows the time evolution of the peak error velocity for the first 20 days of integration with the second, forth, and sixth-order ordinary schemes. The peak error velocity fluctuates rapidly during the first few days integration. After the 5 days of integration, the peak error velocity show the decaying inertial oscillation superimposed into asymptotic values. The asymptotic value is around 0.19 cm/s for the ordinary scheme and 0.15 cm/s for the compact scheme. For the sixth order difference, the asymptotic value is near 0.04 cm/s for the ordinary scheme and 0.02 cm/s for the compact scheme.

Figure 8
Peak error velocity for the second, fourth, and sixth order schemes (from Chu and Fan, 1997a).

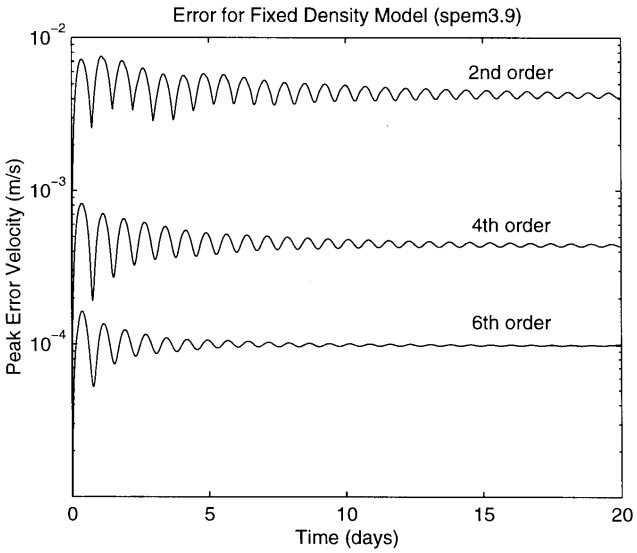

5. Conclusions

The difference between commonly used NSCAT and NCEP surface wind data is not negligible. Root-mean-square difference over the South China Sea increases from 3.6 m/s 1 November to a maximum value of 6.7 m/s on 4 November 1996, the day when Ernie was formed; and then fluctuates between 6.7 m/s and 2.7 m/s afterwards. The response of the South China Sea to the uncertain surface forcing is also evident. Therefore, it is quite urgent to study the role of boundaries and sensitivity to boundary conditions.

The optimization method provides a useful scheme to obtain unknown open boundary values from known interior values. Different from the adjoint method, this scheme can be easily incorporated into any ocean models. For time-dependent dynamical models, when the temporally varying values are given at interior observation points, the optimization method can be used for each time step to obtain the unknown open boundary values for that time step. For a primitive equation model with turbulent mixing processes (e.g., POM), it is very important to use smoothing on the open boundary parameter vector. The optimization method performs well even when random noises are added to the 'observational' points. This indicates that we can use real-time data to invert for the unknown open boundary values.

The σ-coordinate, pressure gradient error depends on the choice of difference schemes. By choosing an optimal scheme, the error may be reduced a great deal without increasing the horizontal resolution. Analytical analysis shows that the truncation error of the fourth-order scheme may be 1-2 order of magnitude smaller than the second-order scheme, and the truncation error of the sixth-order scheme may be 1-2 order of magnitude smaller than the fourth-order scheme within the same order of the difference the combined compact scheme leads to a minimum truncation error. The compact scheme may reduce near 55% error, and the combined compact scheme may reduce near 84% error for the sixth order difference.

Acknowledgments

This research is sponsored by the Office of Naval Research (ONR) Naval Ocean Modeling Program (NOMP). Chenwu Fan, Shihua Lu, and Yuchun Chen have contrib-

uted significantly to these studies of toward accurate littoral zone modeling.

Biography

Peter Chu, an associate professor at the Naval Postgraduate School, received a Ph.D. from the University of Chicago in 1985. A long term objective of his research is the ocean analysis and prediction.

REFERENCES

Beckmann, A., and D. B. Haidvogel, 1993: Numerical simulation of flow around a tall isolated seamount. Part 1: Problem formulation and model accuracy. Journal of Physical Oceanography, 23, 1736-1753.

Blumberg, A.F., and G.L. Mellor, 1987: A description of a three-dimensional coastal ocean circulation model. In: Three Dimensional Coastal Ocean Models, edited by N.S. Heaper, American Geophysical Union, 1-16.

Chang, H.R., and H.N. Shirer, 1985: Compact spatial differencing techniques in numerical modeling. Monthly Weather Review, 113, 409-423.

Chapman, D., 1985: Numerical treatment of cross-shelf open boundaries in a barotropic ocean model. Journal of Physical Oceanography, 15, 1060-1075.

Chu, P.C., Y.C. Chen, and S.H. Lu, 1998a: On Haney-type surface thermal boundary conditions for ocean circulation models. Journal of Physical Oceanography, 28, 890-901.

Chu, P.C., Y.C. Chen, and S.H. Lu, 1998b: Evaluation of Haney-type surface thermal boundary conditions using a coupled air-ocean model. Journal of Oceanography, in revision.

Chu, P.C., and C. Fan, 1997a: Sixth-order difference scheme for sigma coordinate ocean models. Journal of Physical Oceanography, 27, 2064-2071.

Chu, P.C., and C. Fan, 1997b: Compact difference scheme for sigma coordinate coastal ocean models. International Journal for Numerical Methods in Fluids, submitted.

Chu, P.C., and C. Fan, 1998: A three-point combined compact difference scheme. Journal of Computational Physics, 140, 1-30.

Chu, P.C., C. Fan, and L. Ehret, 1997: Determination of open boundary conditions with an optimization method. Journal of Atmospheric and Oceanic Technology, 14, 723-734.

Chu, P.C., S.H. Lu, and W.T. Liu, 1998: Uncertainty of the South China Sea prediction using NSCAT and NCEP winds during tropical storm Ernie 1996. Journal of Geophysical Research, submitted.

Gunson, J.R., and P. Malanotte-Rizzoli, 1996: Assimilation studies of open-ocean flows: 1. estimation of initial and boundary conditions. Journal of Geophysical Research, 101, 28,457-28,472.

Haidvogel, D.B., J.L. Wikin, and R. Young, 1991: A semi-spectral primitive equation model using vertical sigma and orthogonal curvilinear coordinates. Journal of Computational Physics, 94, 151-185.

Haney ,1991: On the pressure gradient force over steep topography in sigma coordinate ocean models. Journal of Physical Oceanography, 21, 610-619.

Hedstrom, K., 1994: User's Manual for a Semi-Spectral Primitive Equation Ocean Circulation Model Version 3.9, Rutgers University, New Jersey.

McCalpin, J.D., 1994: A comparison of second-order and fourth-order pressure gradient algorithms in a sigma-coordinate ocean model. International Journal for Numerical Methods in Fluids, 18, 361-383.

Mellor, G.L., T. Ezer, and L.-Y. Oey, 1994: The pressure gradient conundrum of sigma coordinate ocean models. Journal of Atmospheric and Oceanic Technology, 11, 1126-1134.

Mellor, 1991: User's Guide for A Three Dimensional, Primitive Equation, Numerical Ocean Model. Princeton University.

Oliger, J., and Sundstrom, 1978: Theoretical and practical aspects of some initial boundary value problems in fluid dynamics. SIAM Journal of Applied Mathematics, 35 (3), 419-446.

Orlanski, I., 1976: A simple boundary condition for unbounded hyperbolic flows. Journal of Computational Physics, 21, 251-269.

Robinson, A.R., 1993: Physical precesses, field estimation and interdisciplinary ocean modeling. Harvard Open Ocean Model Reports, Harvard University, Cambridge, 71 pp.

Seiler, U., 1993: Estimation of the open boundary conditions with the adjoint method. Journal of Geophysical Research, 98, 22855-22870.